

# A Terminal Area PBL Prediction System at Dallas–Fort Worth and Its Application in Simulating Diurnal PBL Jets



Michael L. Kaplan, Yuh-Lang Lin, Joseph J. Charney, Karl D. Pfeiffer, Darrell B. Ensley, David S. DeCroix,\* and Ronald P. Weglarz  
Department of Marine, Earth, and Atmospheric Sciences,  
North Carolina State University, Raleigh, North Carolina

## ABSTRACT

A state-of-the-science meso- $\beta$ -scale numerical weather prediction model is being employed in a prototype forecast system for potential operational use at the Dallas–Fort Worth International Airport (DFW). The numerical model is part of a unique operational forecasting system being developed to support the National Aeronautics and Space Administration's (NASA) Terminal Area Productivity Program. This operational forecasting system will focus on meso- $\beta$ -scale aviation weather problems involving planetary boundary layer (PBL) turbulence, and is named the Terminal Area PBL Prediction System (TAPPS). TAPPS (version 1) is being tested and developed for NASA in an effort to improve 1–6-h terminal area forecasts of wind, vertical wind shear, temperature, and turbulence within both stable and convective PBLs at major airport terminal areas. This is being done to enhance terminal area productivity, that is, aircraft arrival and departure throughput, by using the weather forecasts as part of the Aircraft Vortex Spacing System (AVOSS). AVOSS is dependent upon nowcasts or short-period forecasts of wind, temperature, and eddy dissipation rate so that the drift and dissipation of wake vortices can be anticipated for safe airport operation. This AVOSS system will be demonstrated during calendar year 2000 at DFW.

This paper describes the numerical modeling system, which has three basic components: the numerical model, the initial data stream, and the postprocessing system. Also included are the results of several case study simulations with the numerical model from a field program that occurred in September 1997 at DFW. During this field program, detailed local measurements throughout the troposphere, with special emphasis on the PBL, were taken at and surrounding DFW in an effort to verify the numerical model simulations. Comparisons indicate that the numerical model is capable of an accurate simulation of the vertical wind shear structure during the diurnal evolution of the PBL when compared directly to specific local observations. The case studies represent unambiguous examples of the dynamics of the Great Plains diurnal low-level jet stream. This diurnal jet stream represents the dominant low-level wind shear–production mechanism during quiescent synoptic-scale flow regimes. Five consecutive daily case studies, during which this phenomenon was observed over and in proximity to DFW, are compared to the products derived from TAPPS.

## 1. Introduction

During instrument meteorological flight conditions, air traffic control (ATC) sets the spacing for

departing and arriving aircraft in order to avoid unsafe encounters with aircraft wake vortices. The current flight rules are conservatively based on aircraft weight categories and do not consider weather conditions. During visual meteorological conditions, pilots are able to accept responsibility for spacing behind the leading aircraft by assessing the wake relevance based on actual conditions, and frequently follow at closer distances than ATC would be required to provide. The spacing could be reduced during instrument approaches as well *if weather were considered*, since crosswinds can transport wake vortices out of the flight

---

\*Current affiliation: Los Alamos National Laboratory, Group TSA-4, Los Alamos, New Mexico.

Corresponding author address: Yuh-Lang Lin, Department of Marine, Earth, and Atmospheric Sciences, Box 8208, North Carolina State University, Raleigh, NC 27695-8208.

E-mail: yl\_lin@ncsu.edu

In final form 7 February 2000.

corridor and wake vortices can decay according to the level of atmospheric turbulence (e.g., Proctor 1998). A system to safely reduce aircraft separation for the purpose of increasing airport capacity is under development by the National Aeronautics and Space Administration's (NASA) Terminal Area Productivity (TAP) Program. This system, called the Aircraft Vortex Spacing System (AVOSS), is described in Hinton (1995, 1996), Perry et al. (1997), Kaplan et al. (1999), and Hinton et al. (1999), and incorporates wake vortex observations, wake vortex decay and transport algorithms, the observed and predicted weather state, and system integration. A concept demonstration of the system is planned for Dallas–Fort Worth (DFW) International Airport in 2000. The motivation behind the development of this system is the need for increased airport capacity while maintaining the present level of safety. Means of safely increasing airport capacity will be a critical issue as the number of flights to and from U.S. airports increases substantially in the near future.

As part of the weather component of AVOSS, a state-of-the-science numerical weather prediction model named the Terminal Area PBL Prediction System (TAPPS) is being developed. Forecast products generated by TAPPS, such as vertical profiles of wind, temperature, turbulent kinetic energy (TKE), and eddy dissipation rate (EDR) may allow AVOSS to anticipate changes in aircraft spacing due to evolving weather conditions. Presently, the TAPPS model and the value of its products for AVOSS are being evaluated within a meso- $\beta$ -scale region centered on DFW. The TAPPS model is an extension of the Mesoscale Atmospheric Simulation System (MASS). MASS is one of many mesoscale or regional-scale numerical weather prediction models being run in both real-time and experimental modes at universities in an effort to support government or privately funded applied research projects (e.g., Manobianco et al. 1996; Mass and Kuo 1998).

In the following sections of this paper we will first provide an overview of TAPPS version 1 (TAPPS-1) emphasizing 1) the history of the MASS model, 2) the MASS model configuration employed in real time, and 3) the postprocessing system that has been developed to provide numerical products to AVOSS. The results of verification studies of several simulation experiments against a prototype version of this prediction system will then be presented. Five consecutive case studies of diurnal PBL jet formation observed by a network of rawinsonde and surface-based observing systems during September 1997 in and around DFW

will be addressed. In addition to showing examples of TAPPS products, we will focus on the ability of the numerical model to predict diurnal PBL jet structure at several locations as well as reproducing the fundamental dynamics of diurnal PBL jet evolution.

## 2. Components of TAPPS version 1

In this section, the components of the existing version of TAPPS (TAPPS-1) and the upgrades anticipated to be present in TAPPS version 2 (TAPPS-2) are described. Both TAPPS-1 and TAPPS-2 are anticipated to be tested by calendar year 2000 in support of the AVOSS demonstration at DFW.

### a. NASA's development of the MASS model

The numerical simulation model, which forms the centerpiece of TAPPS, is MASS. MASS has been employed for nearly 20 years by NASA and other government agencies for use in a wide variety of basic research, applied research, and operational support programs. MASS was originally funded by NASA Headquarters for the purpose of severe storm research in the early–middle 1980s by scientists at the NASA Goddard Space Flight Center (e.g., Kaplan et al. 1982a,b, 1984; Koch et al. 1983; Koch 1985; Kocin et al. 1984, 1985; Zack and Kaplan 1987). During the spring of 1982 the model was run in real time for an experiment involving 30 case studies to predict severe weather, and was evaluated in comparison to the then operational National Weather Service (NWS) Limited Area Fine Mesh Model (LFM) model by NASA and National Oceanic and Atmospheric Administration (NOAA) scientists at the National Severe Storms Laboratory (NSSL) (Koch et al. 1985).

The MASS model was subsequently utilized to support several NASA operational programs during the 1982–88 time frame. These programs included 1) the NASA Langley Global Tropospheric Experiment, 2) NASA Kennedy Space Center summer launches (Kaplan et al. 1983), 3) the NASA Langley aviation lightning research program, and 4) the Genesis of Atlantic Lows multiagency research program. During this period, the MASS model was also employed for extensive basic and applied research undertaken by NASA, including research into the processes responsible for the development of the Presidents' Day cyclone (Uccellini et al. 1987; Uccellini 1990; Whitaker et al. 1988), the assimilation of satellite data into mesoscale models (Cram and Kaplan 1985), and

the meteorological conditions that contributed to the Shuttle *Challenger* disaster (Uccellini et al. 1986).

Recently, MASS has been employed to test the utility of the NOAA wind profiler datasets (Cram et al. 1991), in the assimilation of satellite data into mesoscale models (Manobianco et al. 1991, 1992, 1994), to determine the role of terrain in severe weather development (Kaplan and Karyampudi 1992a,b), and to understand the processes contributing to severe weather development over the southeastern United States (Hamilton et al. 1998; Kaplan et al. 1995, 1997, 1998; Koch et al. 1998).

MASS is currently being utilized in a real-time mode at the Department of Marine, Earth, and Atmospheric Sciences at North Carolina State University in support of joint private/NWS/university experimental forecasting research. Furthermore, MASS has been utilized in support of the Applied Meteorological Unit at the NASA Kennedy Space Center in both a research and real-time mode (e.g., Manobianco et al. 1996; Bauman et al. 1997).

#### *b. MASS model in TAPPS-1*

The version of MASS currently employed in TAPPS1, version 5.10, is described in Table 1 and represents an updated version published by MESO, Inc. (1995). The model is integrated in space and time over a coarse mesh matrix of  $60 \times 60 \times 56$  grid points within which is nested a fine mesh matrix of  $60 \times 60 \times 56$  grid points on a standard computer workstation (Figs. 1a,b). The horizontal resolutions at the latitude of DFW is  $\sim 24$  km for the outer coarse mesh grid and is  $\sim 12$  km for the inner fine mesh grid. The vertical layers within the model, which are depicted in Table 2, cover the atmosphere from about 5 m above the earth's surface to about 16 000 m in elevation. The vertical spacing in between model surfaces increases with elevation above the earth's surface so that detailed vertical resolution exists within the PBL, particularly below 100 m with 10 model levels within this layer.

The coarse mesh simulations are initialized from the National Weather Service Eta Model analyses valid at 0000 and 1200 UTC. The coarse mesh model is integrated for 24 h of real time. The fine mesh model is initialized from the interpolated coarse mesh simulations valid at 1500 and 0300 UTC. The fine mesh model is integrated for 21 h of real time. This allows the entire 24-h daily period to be covered with 12-km real-time forecast fields for the purpose of AVOSS product generation.

---

TABLE 1. Characteristics of the MASS model version 5.10 (source: MESO Inc.).

---

#### **Numerics:**

- 1) Hydrostatic primitive equation model
- 2) 3D primitive equations for  $u$ ,  $v$ ,  $T$ ,  $q$ , and  $p$
- 3) Cartesian grid superimposed on a polar stereographic map image plane
- 4)  $\sigma_p$ -normalized terrain-following vertical coordinate system (Kaplan et al. 1982a)
- 5) Vertical coverage from  $\sim 10$  to  $\sim 16$  000 m
- 6) Energy-absorbing sponge layer near model top
- 7) Fourth-order horizontal space differencing on an unstaggered grid
- 8) Split-explicit time integration schemes: (a) forward-backward for the gravity mode and (b) Adams-Bashforth for the advective mode (Mesinger and Arakawa 1977; Mesinger 1977)
- 9) Piecewise parabolic method for scalar advection
- 10) Time-dependent lateral boundary conditions
- 11) Positive-definite advection scheme for the advection of scalar dependent variables (Carpenter et al. 1988)

#### **Initialization scheme:**

- 1) First guess provided by large-scale gridded analyses from the Meso-Eta
- 2) Reanalysis of rawinsonde, surface, and asynoptic (radar, satellite, and/or profiler-derived data) using a 3D optimum interpolation scheme
- 3) 10-km terrain database derived from observations
- 4) 10-km satellite or climatological sea surface temperature database
- 5) 10-km land use classification scheme (Anderson et al. 1976)
- 6) 10-km climatological subsoil moisture database derived from antecedent precipitation (Anderson et al. 1976; Noilhan and Planton 1989)
- 7) 10-km normalized difference vegetation index

#### **PBL specification:**

- 1) Blackadar PBL scheme (Blackadar 1979; Zhang and Anthes 1982)
- 2) Surface energy budget (Mahrt and Pan 1984)
- 3) Soil hydrology scheme (Mahrt and Pan 1984)
- 4) Atmosphere radiation attenuation scheme (Mahrt and Pan 1984)

#### **Moisture physics:**

- 1) Grid-scale prognostic equations for cloud water and ice, rainwater, and snow (Lin et al. 1983)
  - 2) Kuo-MESO subgrid-scale convective parameterization scheme (MESO Inc. 1995)
-

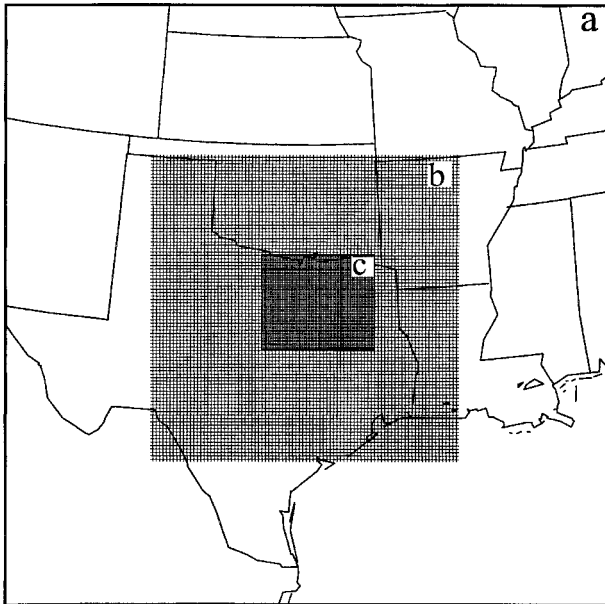


FIG. 1. (a) TAPPS coarse mesh grid region employed in the 24-km DFW deployment simulations. (b) TAPPS fine mesh grid region employed in the 12-km DFW deployment simulations. (c) Projected ultrafine mesh grid region to be employed in the 6-km TAPPS-2 system scheduled for operation in calendar year 2000.

### c. Initial data stream

The existing operational gridded data stream used to initialize TAPPS-1 is simply the Meso-Eta analyses (Rogers et al. 1996). Since rawinsonde and surface data are already included in this analysis, no dynamic initialization scheme is employed at the present time.

Lateral boundary conditions for the coarse mesh grid are derived from the Meso-Eta forecast fields and are updated every 6 h. Lateral boundary conditions for the fine mesh nested grid are derived from the coarse mesh grid by employing a one-way algorithm that uses weighted temporal and spatial smoothing of dependent variables from the two grids (Davies 1976). The fine mesh nested grid is initialized from the cubic spline-interpolated dependent variables that were generated on the coarse mesh grid.

Several modifications to the initialization are planned for the next version of TAPPS in order to supply higher-resolution simulations and additional data for peak traffic times at DFW. These modifications will be tested for use in support of the AVOSS year 2000 demonstration. The TAPPS-2 version will be initialized every 6 h with shorter-period 9-h simulations, and will be run over a finer horizontal grid resolution of about 6 km (Fig. 1c). The asynoptic initial conditions will include wind and height data derived from

the NOAA midcontinental operational wind profiler network. The height data will be derived from the wind data by employing a technique dependent upon the velocity divergence equation (Cram et al. 1991). The 12-km simulation will serve as the first guess for the TAPPS-2 initial conditions. These gridded forecast fields will then be modified by the inclusion of profiler-derived winds and heights generated from an optimal interpolation analysis scheme (Daley 1992). Also included will be available surface aviation and mesonet observations as well as other available asynoptic rawinsonde soundings. Satellite and radar-derived relative humidity fields will be incorporated into the initial data stream employing a technique described in Zack et al. (1988). Experiments will be performed prior to the implementation of TAPPS-2 to determine whether a reanalysis technique such as incremental analyses updates of the asynoptic data (e.g., Young and Zack 1998) or a nudging procedure (e.g., Stauffer and Seaman 1990) produces the most improved shorter-period forecasts.

### d. Postprocessing system

The suite of products required for AVOSS are quite specific. Vortex drift and dissipation are the main problems that affect airport productivity in that the dynamics of these vortices dictate the safe spacing between departing and landing aircraft. The goal of the TAP program is to maintain the throughput rate of aircraft as airport capacity increases and to accomplish this *independent* of weather conditions. This increase in airport capacity is anticipated to be quite substantial during the early part of the twenty-first century. In an effort to meet the needs of increased capacity, better 1–6-h terminal area predictive information is necessary so that AVOSS can determine the rate of vortex transport through the approach and departure corridors. Vortex drift through the approach and departure corridors is strongly controlled by the magnitude of the cross-runway wind velocity component. Since the major runways at DFW are aligned in the north–south direction so that aircraft can take off and land in the same direction as the prevailing winds, the  $u$  component of the horizontal wind in the model represents the cross-runway wind. The postprocessor produces time sections and vertical soundings up to 1000-m elevation at DFW of  $u$  wind velocity component from the 12-km simulation based on 15-min simulated values. Also produced are the headwind ( $v$  wind velocity component), variance of both wind velocity components, relative humidity, and virtual

TABLE 2. The vertical structure of the 3D numerical model with the number of half-sigma levels, sigma values ( $\sigma$ ) at half-sigma levels, approximate pressure ( $p$ , in hPa) at sigma levels, and the approximate difference in height between the sigma levels ( $\Delta z$ , in m). Approximate pressure levels are computed based on  $p_s = 1000$  hPa.

Number	$s$	$p$ (hPa)	$\Delta z$ (m)	Number	$s$	$p$ (hPa)	$\Delta z$ (m)
54	0.025	123	1050	27	0.700	730.0	220
53	0.050	145	930	26	0.724	752.0	205
52	0.075	168	825	25	0.748	773.0	190
51	0.100	190	735	24	0.769	792.0	180
50	0.125	213	660	23	0.790	811.0	175
49	0.150	235	600	22	0.810	829.0	165
48	0.175	258	550	21	0.830	847.0	155
47	0.200	280	510	20	0.849	864.0	140
46	0.225	303	475	19	0.868	881.0	130
45	0.250	325	440	18	0.884	896.0	125
44	0.275	348	420	17	0.900	910.0	120
43	0.300	370	400	16	0.915	924.0	110
42	0.325	393	380	15	0.930	937.0	100
41	0.350	415	365	14	0.943	949.0	85
40	0.375	438	350	13	0.957	961.0	70
39	0.400	460	340	12	0.966	969.0	55
38	0.425	483	330	11	0.975	978.0	45
37	0.450	505	320	10	0.981	983.0	35
36	0.475	528	310	9	0.987	988.0	30
35	0.500	550	300	8	0.9909	991.8	25
34	0.525	573	290	7	0.9948	995.3	10
33	0.550	595	280	6	0.9974	997.6	0.5
32	0.575	618	270	5	0.9975	997.7	1
31	0.600	640	265	4	0.9976	997.8	2
30	0.625	663	255	3	0.9977	997.9	5
29	0.650	685	250	2	0.9980	998.2	5
28	0.675	708	235	1	0.9987	998.8	—

potential temperature. The postprocessor also provides expanded resolution information sets below the 100-m elevation, where the vertical resolution in the model

is greatest. All of these variables are employed by AVOSS to determine vortex drift velocity and elevation for different aircraft.

The persistence of wake vortices is a strong function of atmospheric turbulence (e.g., Tombach 1973; Sarpkaya 1998; Han et al. 1999). In an effort to derive PBL turbulence products from TAPPS-1, the postprocessor calculates TKE based on 30-min time averages. In addition, the postprocessor derives on EDR from the TKE equation:

$$\frac{\partial \bar{e}}{\partial t} + \bar{U}_j \frac{\partial \bar{e}}{\partial x} = +\delta_{i3} \frac{g}{\bar{\theta}_v} \overline{(u_i' \theta_v')} - \overline{u_i' u_j'} \frac{\partial \bar{U}_i}{\partial x_j} - \frac{\partial \overline{(u_j' e)}}{\partial x_j} - \frac{1}{\rho} \frac{\partial \overline{(u_i' p')}}{\partial x_i} - \varepsilon, \quad (1)$$

where  $\bar{e}$  represents the TKE and  $\varepsilon$  represents the EDR (Stull 1988). Two approaches are being tested at the present time in the TAPPS-1 postprocessor. One approach relies on similarity theory to calculate the K coefficients for use in determining the EDR as a residual term from the TKE equation (Arya 1988). A second approach involves employing a higher-order TKE equation, analogous to that employed in the model PBL parameterization itself to calculate EDR as a residual term after all of the TKE generation terms have been calculated (Therry and Lacarrere 1983):

$$\varepsilon = C_\varepsilon \bar{e}^{-3/2} / l_\varepsilon, \quad (2)$$

where  $C_\varepsilon$  is a numerical constant and  $l_\varepsilon$  is the dissipation length.

These TKE, EDR, and individual generation terms are then made available in both time–height cross sections and individual sounding formats as products for use in AVOSS analogous to the vortex drift products. Examples of these and all other products will be displayed later in this paper. All computations are performed on a dedicated DEC-ALPHA 600 series workstation that is resident in the Department of Marine, Earth, and Atmospheric Sciences at North Carolina State University. Postprocessed fields are available on file for the AVOSS group at DFW.

### 3. TAPPS diurnal PBL jet simulations at DFW

In this section of the paper we will describe in detail the ability of the model to predict the structure of the stable and convective boundary layers from several consecutive case studies. These case studies occurred during a NASA Langley field deployment held at DFW during September 1997, prior to the implementation of the TAPPS-1 operational system. In our comparison to the detailed observational datasets derived from this deployment, we will emphasize the ability of the model to simulate the mesoscale structure of diurnal PBL jet streams, which can produce substantial vertical changes in the critical cross-runway wind velocity component.

#### a. AVOSS September 1997 field deployment at DFW

During late September of 1997, a field deployment was held at DFW in an effort to gather experimental datasets that could be utilized to diagnose the relationship between aircraft vortex dynamics and atmospheric conditions. The participants in the experiment included personnel from 1) NASA Langley Research Center, 2) MIT Lincoln Laboratory, 3) North Carolina State University, 4) NOAA National Severe Storms Laboratory, 5) National Weather Service—Fort Worth Office, 6) NASA Wallops Space Flight Center, 7) University of Texas at Dallas, and 8) North Texas State University. The instrumentation in the field at and surrounding DFW are presented in Table 3 and addi-

TABLE 3. Instrumentation characteristics at and surrounding DFW.

#### Instrumentation details

##### Instruments:

- 1) Instrumented tower with SAVPAK, barometer, FLUXPAK, radiometer, and SOILPAK sensors between 45 and 5 m
- 2) 915-Mhz profiler/RASS
- 3) Doppler sodars
- 4) Dual lidars
- 5) Loran CLASS sounding balloons

##### Balloon locations and managing bodies:

DFW = X	MIT Lincoln Laboratory
Denton, TX (DEN)	NOAA/NSSL and North Texas State University
Waxahatchie, TX (WAX)	NASA Wallops
Plano, TX (UTD)	NOAA/NSSL and the University of Texas at Dallas
Fort Worth, TX (FWD)	Fort Worth National Weather Service Forecast Office

tional details concerning these sensors can be found in Dasey et al. (1998).

Data from the four sites surrounding DFW as well as the DFW profiler Radio Acoustic Sounding System (RASS) will be employed for the period from 0900 UTC 15 September–0300 UTC 20 September 1997 in the subsequent analyses in this paper. Hourly profiler wind data and RASS temperatures at DFW as well as raob-derived winds, temperatures, and relative humidities at the surrounding four sites for 0000, 0300, 0900, 1200, 1500, and 2100 UTC were archived for the period including 0900 UTC 15 September–0300 UTC 20 September as well as 0900 UTC 22 September–0300 UTC 27 September 1997.

### b. Diurnal PBL jet dynamics

The low-level jet (LLJ) is a ubiquitous phenomenon in the Great Plains region of North America. Many observationally based studies on LLJ frequency and synoptic structure have been published after the pioneering studies of Wexler (1961) and Bonner (1968), including Arritt et al. (1997), Mitchell et al. (1995), and Whiteman et al. (1997). One of the notable deficiencies of these early observational studies was their inability to discriminate between 1) LLJ due to quasigeostrophic circulations such as the low-level return branch flows that were coupled to the mid-upper-tropospheric transverse ageostrophic jet streak circulations (e.g., Uccellini and Johnson 1979) and

2) mesoscale diurnal PBL circulations that derive their genesis from near-surface-based dynamical forcing functions (e.g., Blackadar 1957). The more recent studies of Arritt et al. (1997), Mitchell et al. (1995), and Whiteman et al. (1997) indicate that many, if not most, of the occurrences of LLJ formation, as diagnosed from wind profiler and asynoptic rawinsonde-derived datasets, are much shallower, much more frequent, and much shorter lived than would be expected from quasigeostrophic transverse ageostrophic jet streak circulations.

In particular, the Whiteman et al. (1997) comprehensive study over the Department of Energy–Atmospheric Radiation Measurement (DOE–ARM) asynoptic rawinsonde network in southeastern Kansas and northeastern Oklahoma found that the elevation of maximum frequency of southerly LLJ occurrences was about 450 m above ground level (AGL). Such a shallow maximum, combined with a consistent period of less than 12-h duration with genesis time shortly after sunset and dissipation time shortly after sunrise, unambiguously establish that most Great Plains LLJ occurrences are due to specific PBL-forcing mechanisms. These PBL-forcing mechanisms are, to a large extent, favored during quiescent synoptic-scale weather regimes.

In a pioneering study, Blackadar (1957) determined theoretically that a preferred regime for LLJ development would be after the formation of a noc-

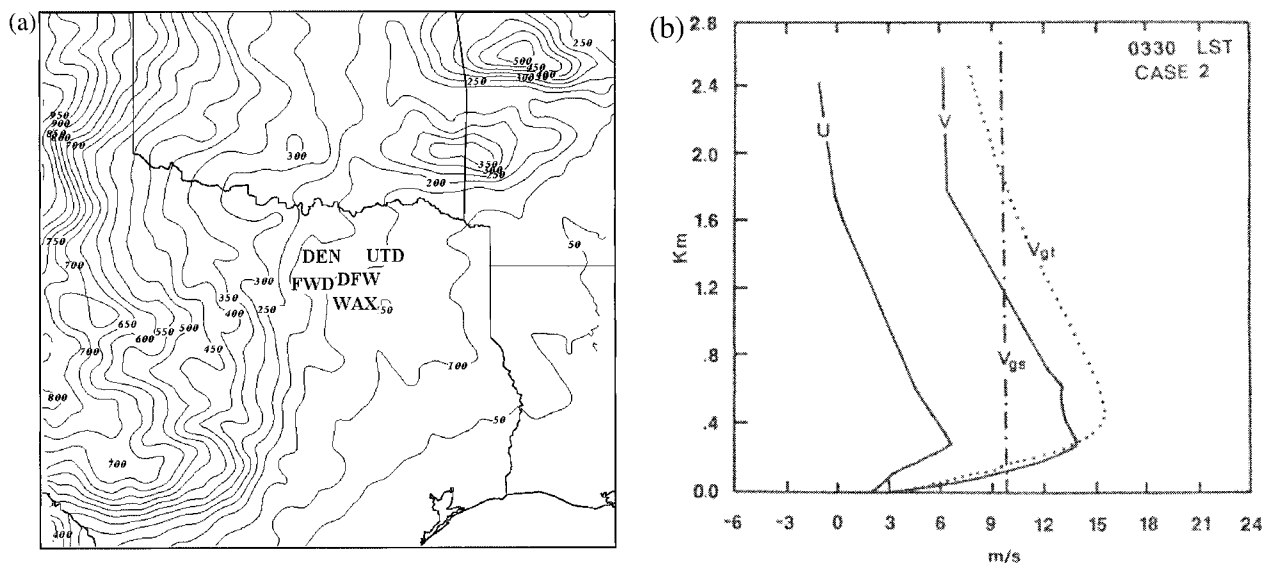
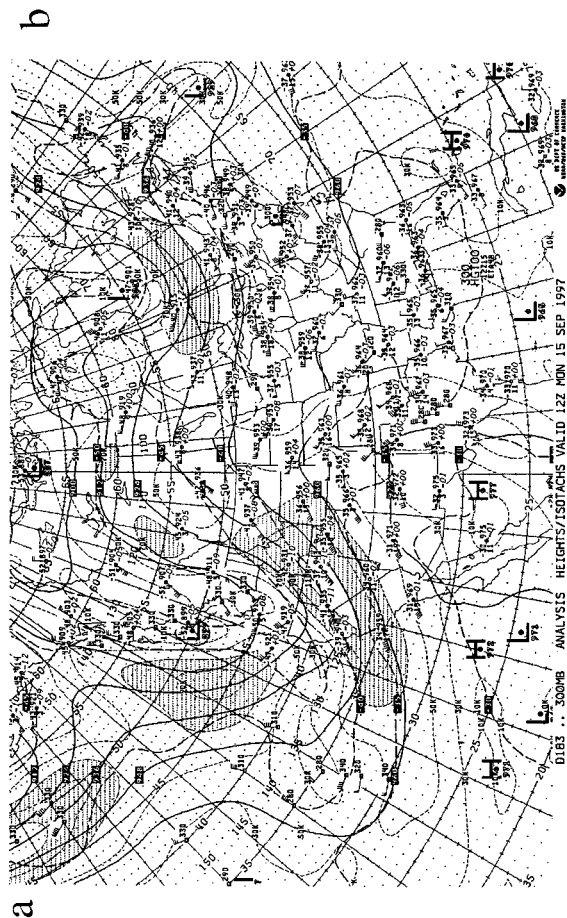
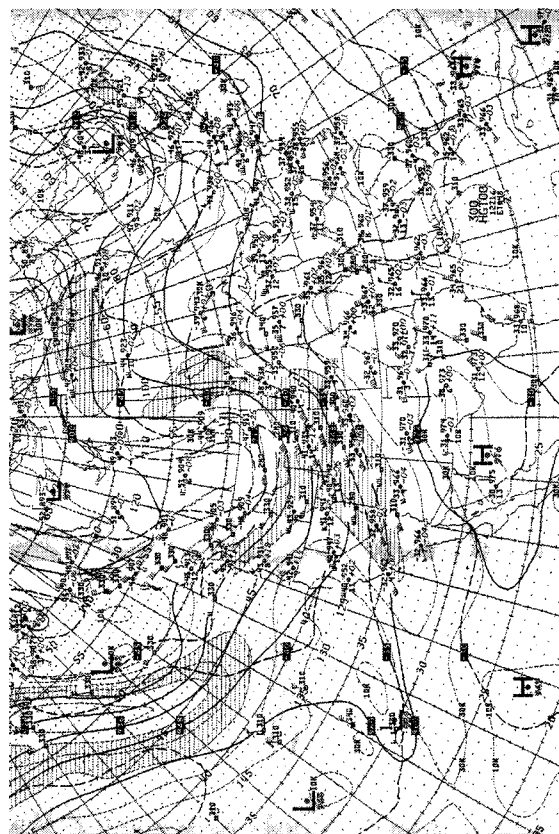


FIG. 2. (a) TAPPS fine mesh terrain (m) and locations of the DFW mesonet rawinsonde observation sites. The contour interval is 50 m, and DFW, FWD, DEN, UTD, and WAX signify the sites at Dallas–Fort Worth International Airport, Fort Worth, Denton, Plano, and Waxahatchie, TX, respectively. (b) Profiles of model-predicted  $u$  and  $v$  components at 0330 LST along with profiles of the total geostrophic component,  $V_{gt}$ , and the synoptic geostrophic component,  $V_{gs}$  (McNider and Pielke 1981).

turnal inversion layer, which typically forms shortly after sunset. This jet stream can develop a significant (for such low elevations) magnitude due in large part to the fact that the inversion acts as an insulating layer, thus reducing the eddy viscosity directly above the inversion. When one considers the Blackadar (1957) findings in conjunction with idealized numerical modeling results such as those from McNider and Pielke (1981), McCorkle (1988), and Fast and McCorkle (1990), which collectively indicate that differential radiative cooling processes near the earth's surface can produce local mesoscale pressure gradients, it is not surprising that during periods of quiescent synoptic-scale flow local shallow diurnally forced jets may be present immediately above a stable PBL. Such features can be extremely important to AVOSS in that they tend to produce strong vertical wind shears and diminished turbulence close to the earth's surface where aircraft-generated vortices are most prevalent and important. The forecasting of wake vortex drift in these situations is critically important and challenging since the LLJ, which is an inherently mesoscale phenomenon, will force the vortices to move in a direction contrary to the synoptic-scale flow.

A simple conceptual example of this atmospheric structure from an idealized simulation is depicted in Fig. 2b (McNider and Pielke 1981). Their simulations clearly indicate that under statically stable conditions, during the middle of the night, in proximity to sloping terrain, and with weak/moderate background flow, how the  $u$  and  $v$  wind components increase in velocity at  $\sim 300$  m AGL produces a shallow shear zone that is clearly different from the synoptic geostrophic wind shear structure and also different from the local mesoscale geostrophic wind shear structure. Consistent with the MASS model simulations, to be shown in following sections of this paper, these idealized shears indicate that the initial dominance of the southerly or south-southeasterly flow during the early nighttime period is replaced during the subsequent later night period by a progressively stronger south-southwesterly flow as the mesoscale zonal component of the geostrophic wind changes direction from northwestward to northeastward in response to the evolving pressure gradient force vector. Additionally, the sharp  $u$  and  $v$  wind component vertical shear zone, which forms at about 300 m AGL and as depicted in Fig. 2b, occurs just above the simulated idealized low-level inversion.

Furthermore, since LLJ situations are not generally accompanied by significant turbulence, slower dissipation rates and a less predictable residence time for



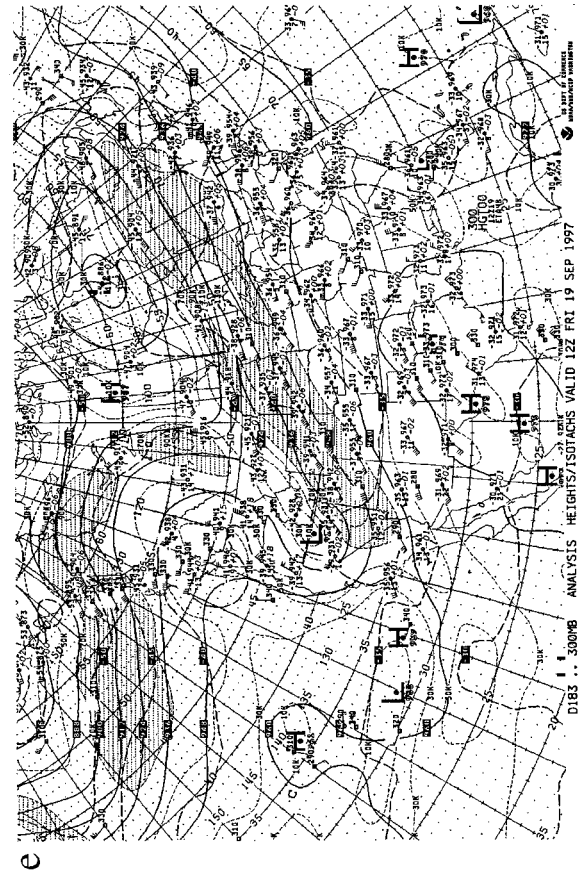
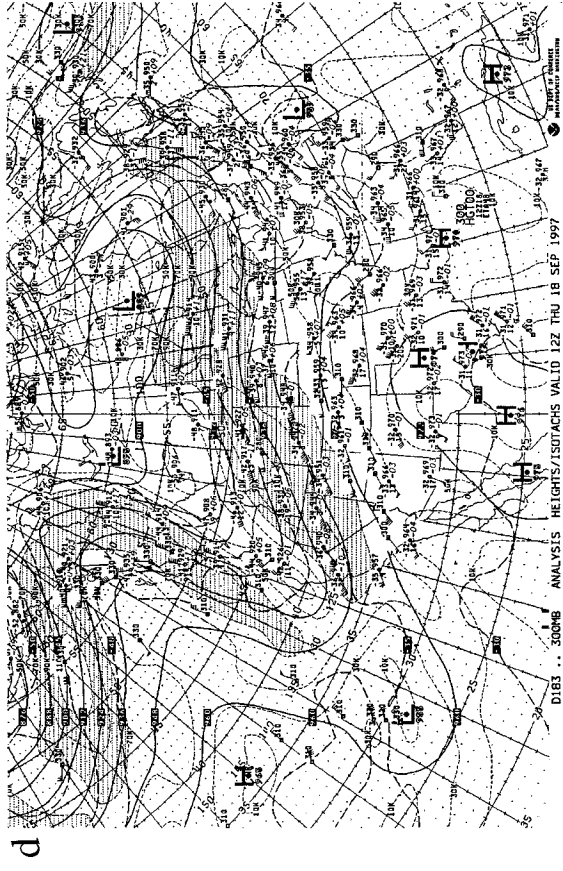
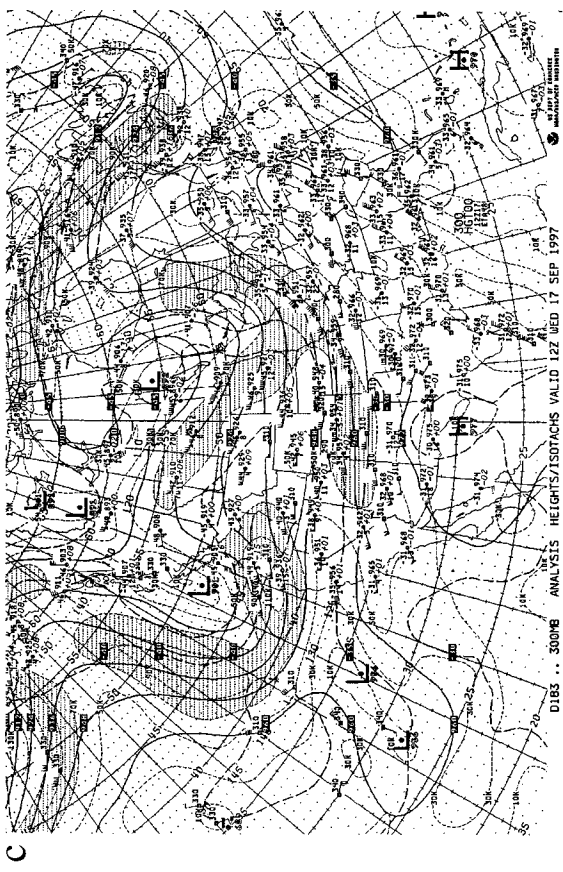


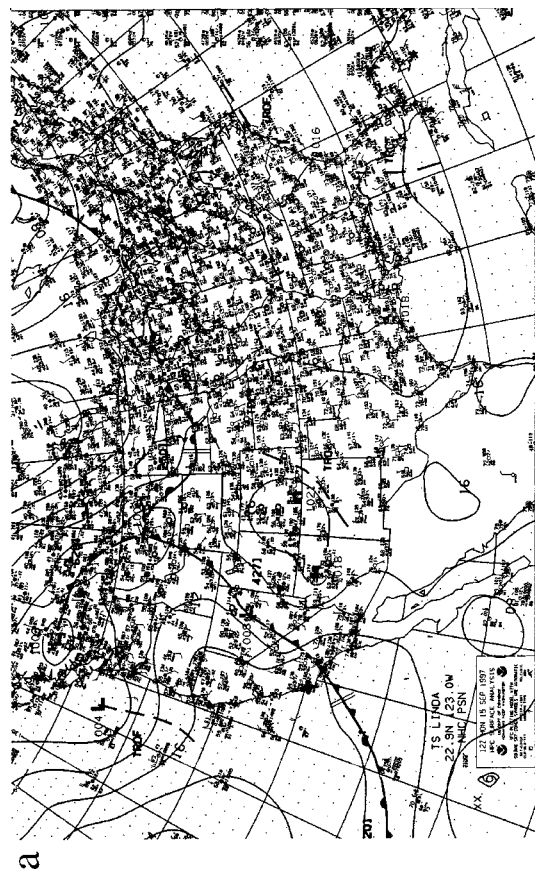
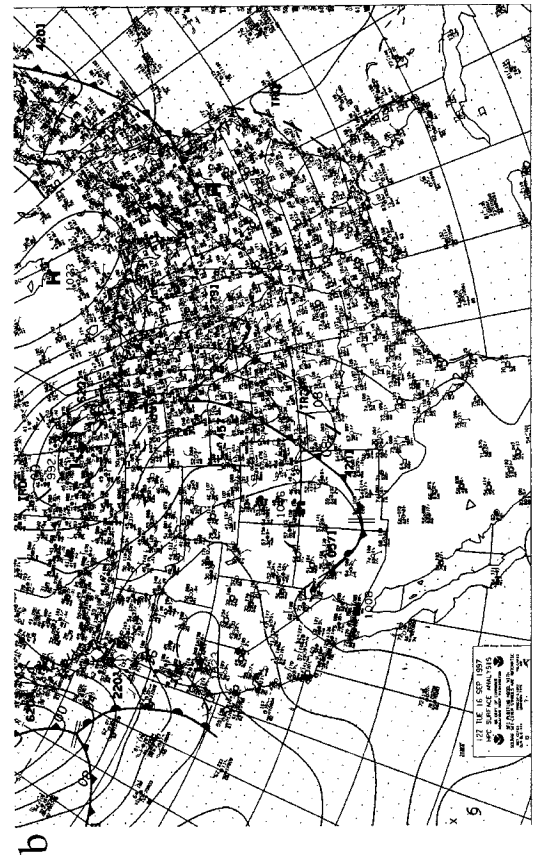
FIG. 3. The National Centers for Environmental Prediction (NCEP) analyzed 300-hPa wind isotachs (small dashed, in  $m s^{-1}$ ), temperature (thick dashed, in  $^{\circ}C$ ), and height (solid, in m), and rawinsonde observations valid at 1200 UTC on (a) 15, (b) 16, (c) 17, (d) 18, and (e) 19 Sep 1997.

the wake vortices would also be manifested. The numerical model can overcome these difficulties by defining the complex vertical wind shears and stability characteristics accompanying the diurnally forced LLJ that would otherwise not be possible to determine from surface-based observations alone. Hence, we will focus on a multiday period during this DFW deployment when diurnally forced PBL jet streams (DPBLJ) were observed in an effort to determine the accuracy of TAPPS in simulating and, hence, predicting these mesoscale phenomena.

*c. Observations of DPBLJ at DFW*

Figure 3 depicts the National Weather Service observed 300-hPa wind, height, and temperature analyses valid at 1200 UTC 15–19 September 1997 over the south-central United States. These analyses, as well as the individual rawinsonde observations from which they were developed, unambiguously define a regime wherein a massive ridge of high pressure aloft remains nearly quasi-stationary over the southern plains. The ridge shows almost no movement, except for a very slow eastward propagation, and is located to the south of a jet streak during this period. As the ridge moves slowly eastward, its tilt becomes oriented progressively more toward the northeast–southwest direction (Fig. 3c) and it strengthens, with 300-hPa heights reaching their maximum value at DFW in excess of 9730 m on 19 September (Fig. 3e). This synoptic situation, typified by a slowly changing high pressure ridge, effectively isolates the region around DFW from any transient disturbances such as synoptic-scale fronts and/or low pressure troughs. The high pressures promote a deep stable layer conducive to clear skies during the day and the development of a strong nocturnal inversion layer at night. The nocturnal inversion is further accentuated by the relatively long nocturnal period during mid–late September. An atmospheric profile with a strong nocturnal inversion is highly conducive to diurnally forced PBL jetogenesis.

The blocking effects of this high pressure ridge can also be inferred from an examination of surface observations at the same time, which are depicted in Fig. 4. During the period of interest, no surface feature is able to propagate into the region surrounding DFW. A quasi-stationary lee trough over extreme western Texas does not move east of the panhandle region (Figs. 4a,b) while a cold front fails to propagate south of Oklahoma during the midweek time period (Fig. 4c). Therefore, the most dominant thermal forcing mechanism at DFW for the entire 5-day pe-



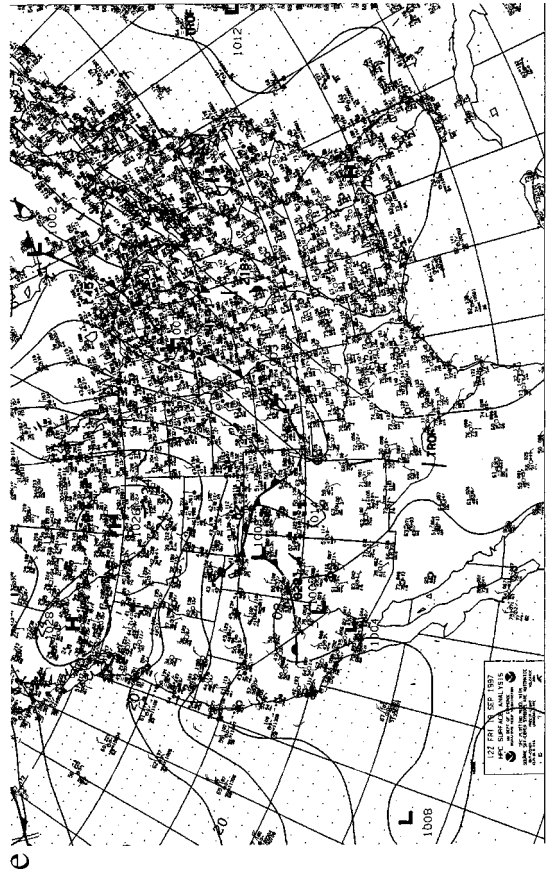
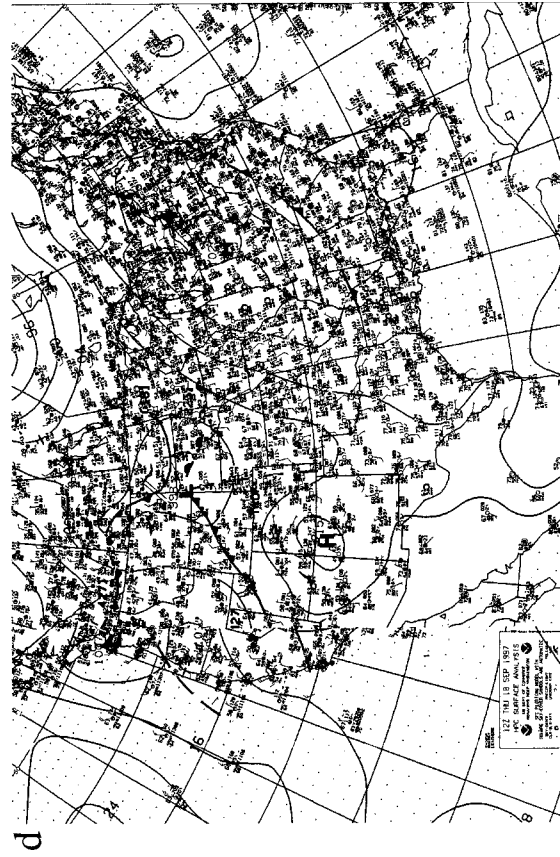
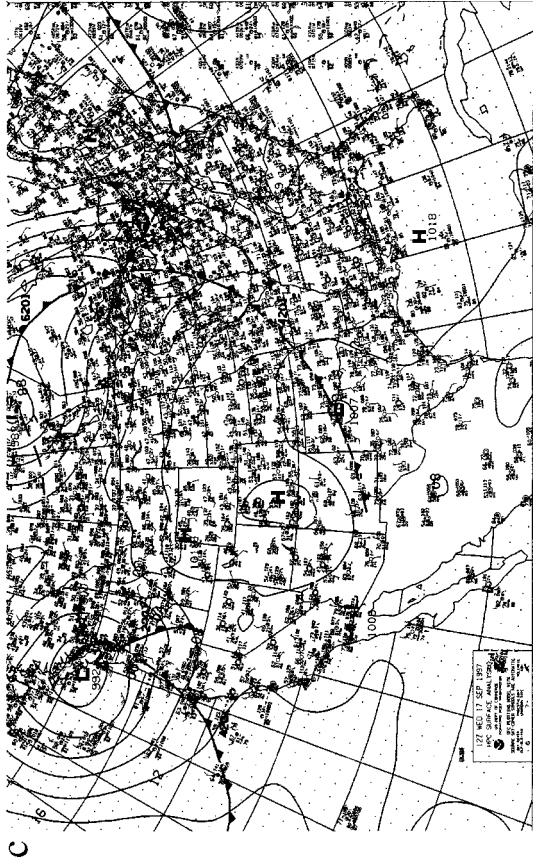


FIG. 4. NCEP-analyzed mean sea level pressure (solid, in mb) and surface observations valid at 1200 UTC on (a) 15, (b) 16, (c) 17, (d) 18, and (e) 19 Sep 1997.

riod is the diurnal temperature cycle, which, in combination with the light background boundary layer wind flow under the deep ridge, promotes ideal conditions for nocturnal jetogenesis processes.

Figures 5–7 depict the observed rawinsonde-derived time sections of virtual potential temperature for the 5-day period at all three deployment rawinsonde stations, Fort Worth (FWD), Denton (DEN), and Waxahatchie (WAX), for which nearly complete records were available. At each location, the diurnal cycle of heating and cooling is similar, with little variation on a daily basis. The most pronounced stable layer

forms shortly after 0600 UTC in between 300 and 400 m AGL, and the inversion, which reaches its peak intensity at about 1200 UTC, is destroyed shortly before 1500 UTC on each day and replaced with a deep, nearly dry-adiabatic layer extending above 1000 m by about 1800 UTC. Note that the diurnal cycle is nearly uniform across the rawinsonde network and during the extended time period.

The dominance of the diurnal cycle is also important for its effects upon the mesoalpha-scale pressure gradient force in the PBL over Texas. Both the formation of the inversion and the subsynoptic-scale pressure gradient force near the inversion are coupled to this diurnal heating and cooling cycle which, in turn, controls the diurnally forced PBL jetogenesis. Figure 8 depicts the mean 24-h temperature range (maximum–minimum observed temperatures), averaged over the 5-day period at every available surface aviation observing station in Texas. Clearly evident is the west-northwest–east-southeast gradient of diurnal change, with maximum values over the elevated plateau near the New Mexico border of about 16°C and minimum values along the immediate Gulf of Mexico coast of about 5°C. The significance of this distribution for the diurnal evolution of the  $u$  wind component lies in the fact that the much larger change over the western high plains compared to the coastal region results in an oscillation of the near-surface pressure gradient force from late afternoon to early morning not unlike a classical mountain–plains solenoidal circulation (e.g., Tripoli and Cotton 1989). Radiation-induced PBL warming maximizes over the western elevated plateau during the late afternoon, creating a region of lower pressure and, therefore, westward-directed tendency in the zonal component of the pres-

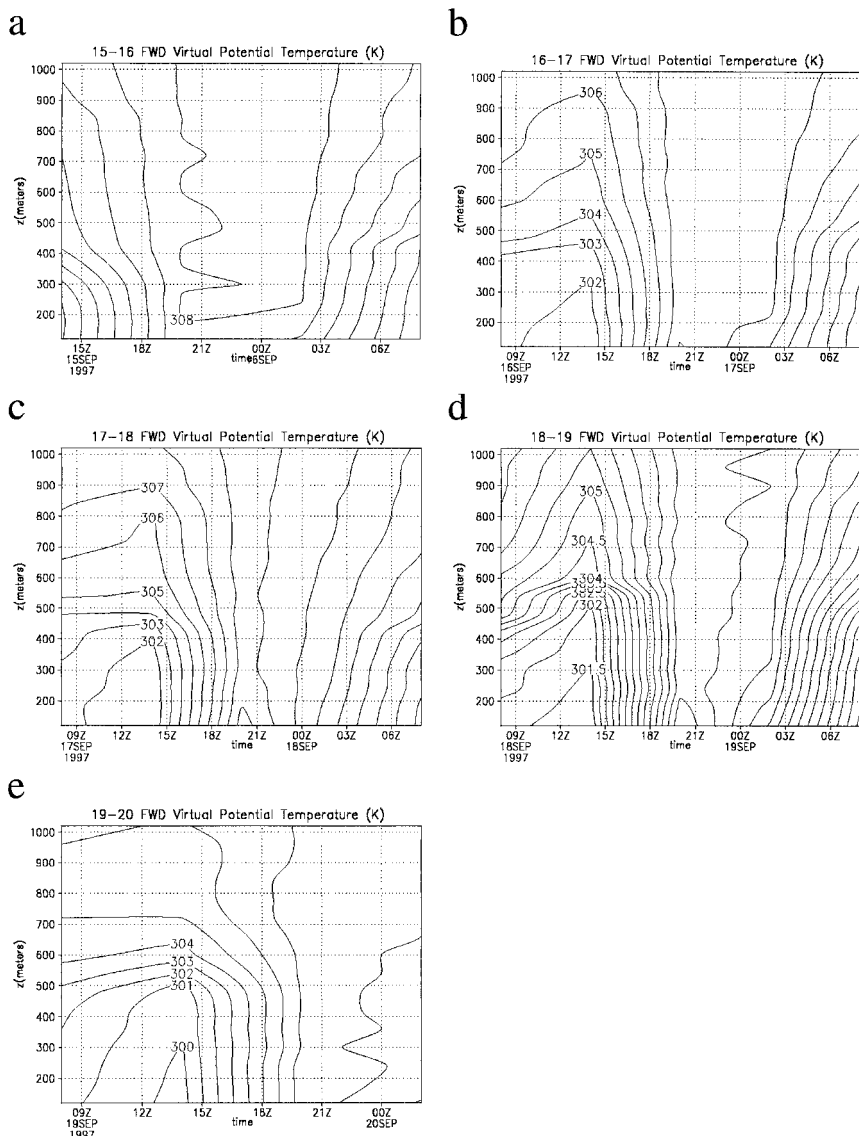


FIG. 5. Fort Worth, TX (FWD), rawinsonde-derived time–height [100–1000 m above mean sea level (MSL)] sections of virtual potential temperature (K) valid for (a) 1400–0800 UTC on 15–16 Sep 1997, 0800–0800 UTC on (b) 16–17 Sep 1997, (c) 17–18 Sep 1997, (d) 18–19 Sep 1997, and (e) 0800–0200 UTC on 19–20 Sep 1997.

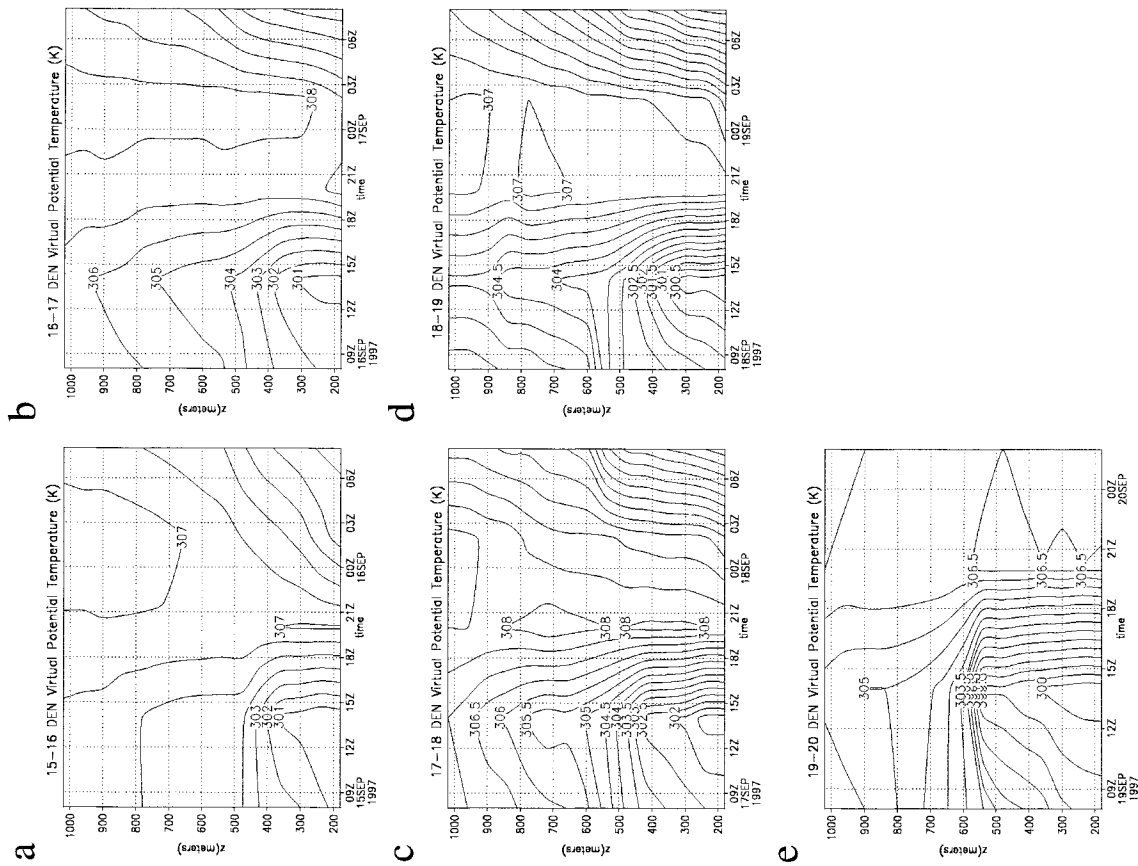


FIG. 6. Denton, TX (DEN), rawinsonde-derived time-height (200–1000 m MSL) sections of virtual potential temperature (K) valid for 0800–0800 UTC on (a) 15–16 Sep 1997, (b) 16–17 Sep 1997, (c) 17–18 Sep 1997, and (d) 18–19 Sep 1997, and (e) 0800–0200 UTC on 19–20 Sep 1997.

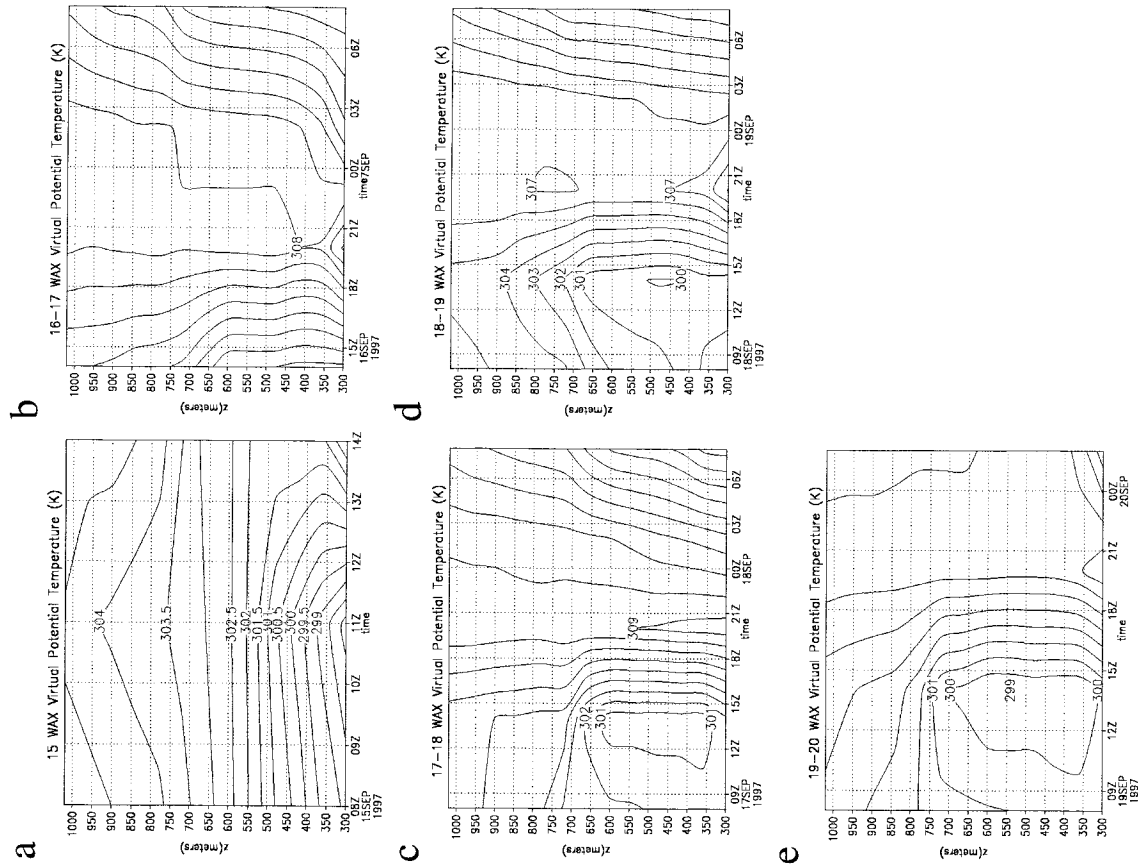


FIG. 7. Waxahatchie, TX (WAX), rawinsonde-derived time-height (300–1000 m MSL) sections of virtual potential temperature (K) valid for (a) 0800–1400 UTC on 15 Sep 1997, (b) 1400–0800 UTC on 16–17 Sep 1997, (c) 0800–0800 UTC on 17–18 Sep 1997, (d) 18–19 Sep 1997, and (e) 0800–0200 UTC on 19–20 Sep 1997.

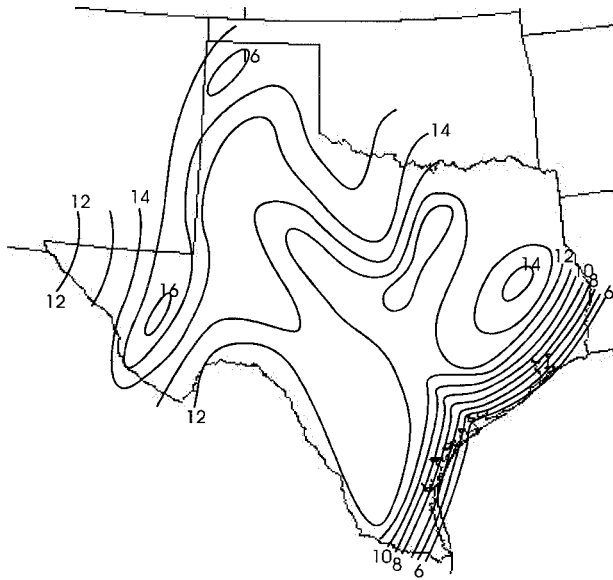


FIG. 8. Observed 5-day mean diurnal variation of surface temperature (in °C) over Texas for 15–19 Sep 1997.

sure gradient force. Conversely, during the late night/early morning period, pressure rises accompanying greater radiational cooling over the western region change the pressure gradient force such that low-level parcels are accelerated more north and eastward than westward.

This diurnal radiation cycle results in the largest magnitude acceleration in the layer of air where friction is weakest—directly above the inversion (Blackadar 1957). The inertial-advective term in the meridional equation of motion is very significant in this process. Since the latitude of DFW is relatively low, the Coriolis force term is relatively small in magnitude, resulting in an inertial response with a period of several hours. Thus, the  $u$  wind velocity component begins to vary in time, reflecting the diurnally varying pressure gradient force. The response of this inertial term in the equations of motion turns the air parcels to the right of the background quasigeostrophic flow. This adjustment process in the meridional and zonal wind velocity fields accelerates air parcels northward and subsequently eastward, in a Lagrangian sense, during the night. The inertial lag effect results in a cross-runway ( $u$ ) wind velocity component cycle that is displaced in time from the period of maximum diurnal surface temperature change due to the differential heating and cooling gradient across Texas. Figures 9–11 depict time sections of the observed cross-runway ( $u$ ) wind velocity component from each deployment rawinsonde location for the 5-day pe-

riod. Figure 12 shows the profiler-derived  $u$  wind velocity component at DFW. These time sections clearly show that the LLJ maximum is located directly above the inversion layer, near 450 m AGL just below which is the maximum of the  $u$  wind velocity component vertical shear. Due to the inertial lag, however, the maximum  $u$  wind velocity component occurs just before 1500 UTC, which is approximately 3 h after the time of minimum surface temperature and strongest low-level inversion formation. The negative maximum in the  $u$  wind velocity component occurs just before 0300 UTC, which is about 12 h out of phase with the positive maximum, reflecting the change in the zonal component of the pressure gradient force above the region surrounding DFW due to the radiational cooling cycle. Also, it is displaced about 3 h from the maximum surface temperature, which occurs between 2100 and 0000 UTC, in agreement with our assertions regarding the local inertial timescale. Furthermore, the negative maxima are about 50% of the absolute value of the positive maxima reflecting the background dominance of an average westerly synoptic-scale wind component of about  $3 \text{ m s}^{-1}$ , with an absolute  $u$  wind velocity component variation of typically on the order of  $12 \text{ m s}^{-1} \text{ day}^{-1}$ , that is, a  $6 \text{ m s}^{-1}$  increase during the morning and a  $6 \text{ m s}^{-1}$  decrease during the evening. The observed DFW region morning lag effect in all of these figures is consistent with the asynoptic rawinsonde observations of Whiteman et al. (1997), who found that the time of the maximum DPBLJ was about 1400 UTC near the 450-m level over southeastern Kansas and northeastern Oklahoma. This lag in the  $u$  wind velocity component maximum is particularly important for airport operations at DFW during the busy morning arrival and departure period, when air traffic increases very rapidly. This is because the runways at DFW are oriented north–south thus rendering vortex dynamics, that is, vortex drift and dissipation, quite vulnerable to slight variations in the  $u$  wind velocity component.

#### d. TAPPS simulations of DPBLJ

Figure 13 depicts the key dynamics accompanying the simulated evolution of DPBLJ for 15 September 1997. The 15th was selected as a representative day although little difference in the simulated and observed dynamics is apparent on the other days. Between 0900 and 1500 UTC at DFW, which tends to be the time period of maximum  $u$  wind velocity component increase over east-central Texas, the pressure gradient

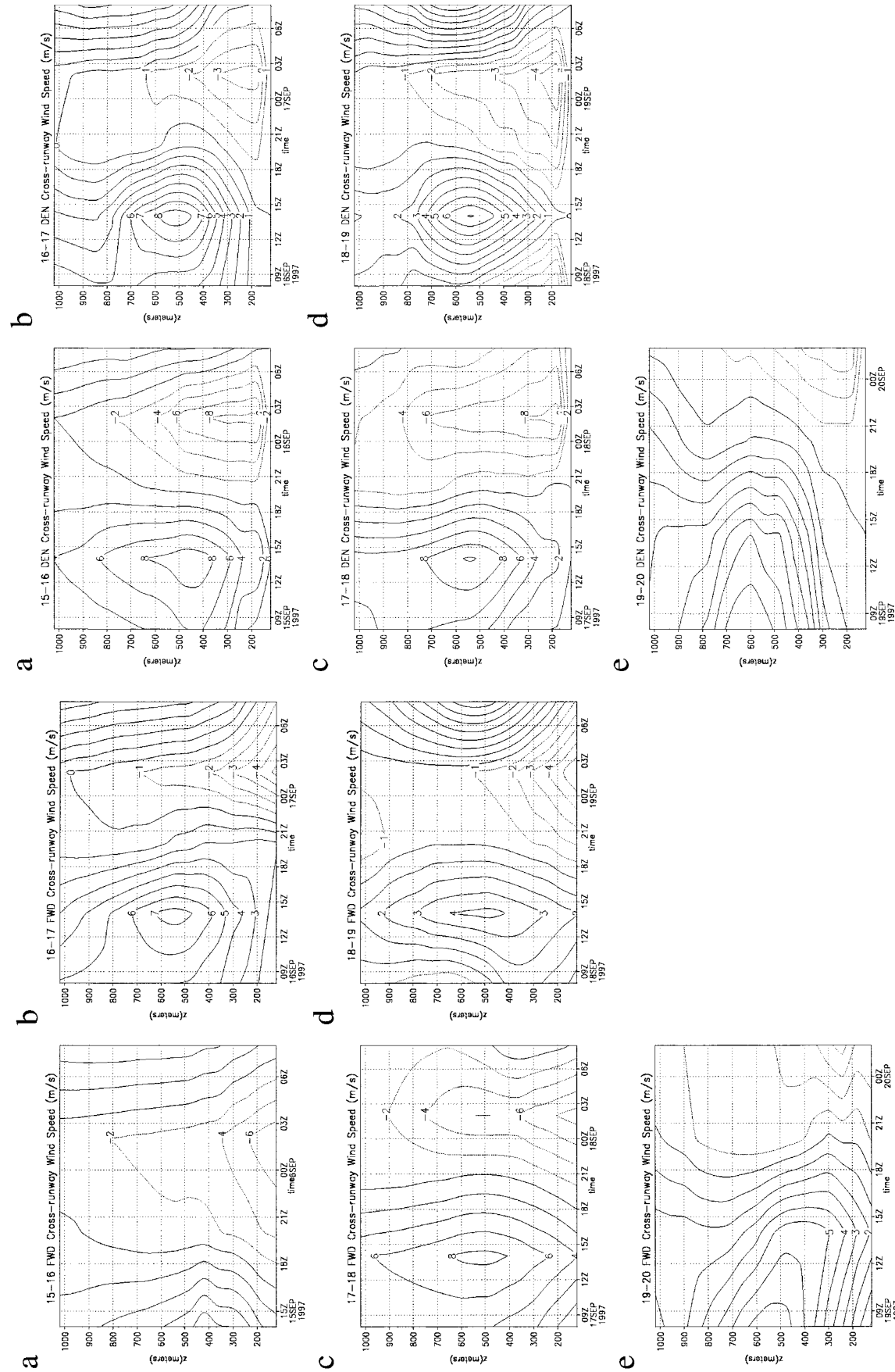


FIG. 9. FWD rawinsonde-derived time-height (100–1000 m MSL) sections of cross-runway ( $u$ ) wind velocity component valid for (a) 1400–0800 UTC on 15–16 Sep 1997, (b) 0800–0800 UTC on 16–17 Sep 1997, (c) 17–18 Sep 1997, (d) 18–19 Sep 1997, and (e) 0800–0200 UTC on 19–20 Sep 1997.

FIG. 10. Same as Fig. 9 except for DEN and except for 0800–0800 UTC on (a) 15–16 Sep 1997, (b) 16–17 Sep 1997, (c) 17–18 Sep 1997, (d) 18–19 Sep 1997, and (e) 0800–0200 UTC on 19–20 Sep 1997.

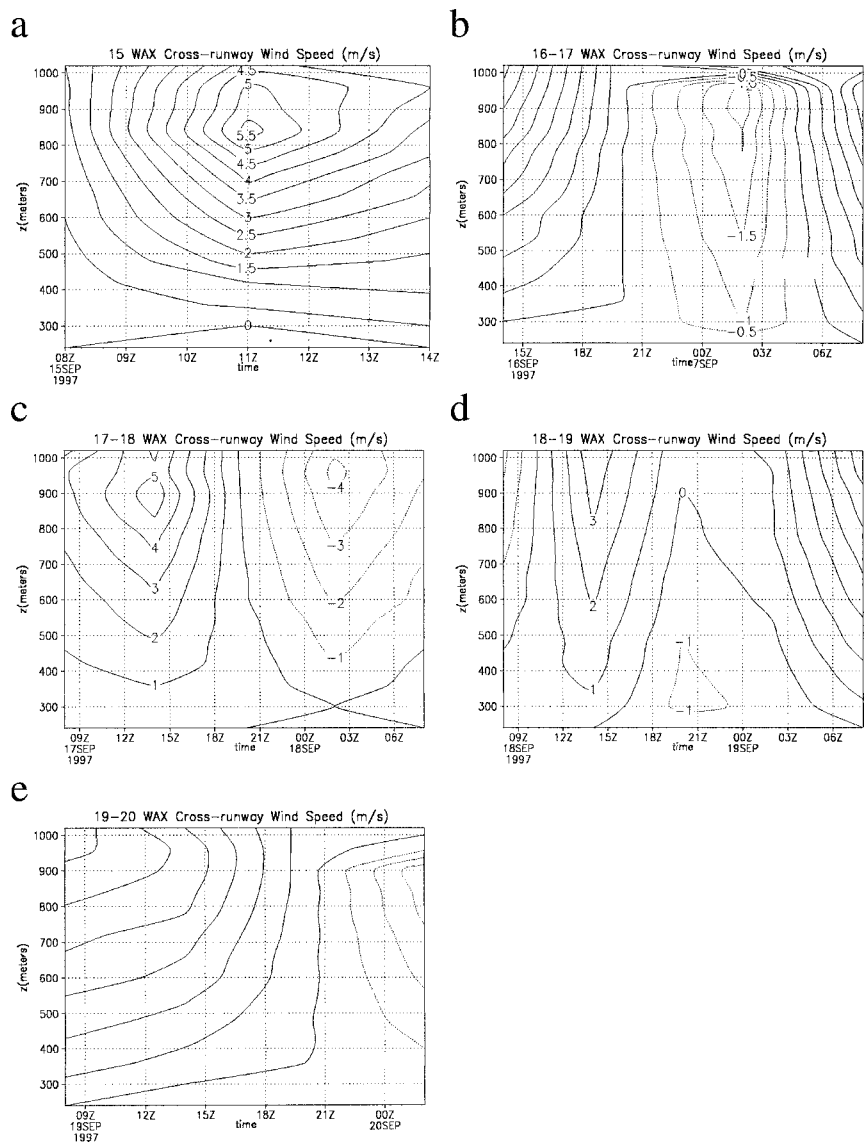


FIG. 11. WAX rawinsonde-derived time–height (200–1000 m MSL) sections of cross-runway ( $u$ ) wind velocity component valid for (a) 0800–1400 UTC on 15 Sep 1997, (b) 1400–0800 UTC on 16 Sep 1997, 0800–0800 UTC on (c) 17–18 Sep 1997, (d) 18–19 Sep 1997, and (e) 0800–0200 UTC on 19–20 Sep 1997.

force shifts from southwestward to northwestward in agreement with the increased radiational cooling over western Texas relative to eastern Texas (Figs. 13a,b). The reduced southward-directed pressure gradient force produces a net acceleration in the northward direction that builds eastward from ABI. The combination of an increasingly northward-directed pressure gradient force and the Coriolis force (above the insulating inversion) directs the winds more toward the east for the period from 0300 to 0900 UTC as can be seen in Figs. 13c,d. The horizontal variation of cooling across central Texas can be determined from a verti-

cal cross section of potential temperature centered on DFW in between Abilene (ABI) and Longview (GGG) at 0300 and 0900 UTC, which is depicted in Figs. 13e,f. The structure of the isentropic surfaces indicates the development of near-surface cooling over the eastern part of the cross section relative to the eastern part. Therefore, the isentropes tilt increasingly downward from west to east at a given height or pressure level, resulting in an alteration in the earlier westward-directed pressure gradient force. The simulated increase in positive zonal wind component is not uniform with height. The flow accelerates most dramatically toward the east-northeast above the near-surface-based inversion, where the eddy viscosity is lower, than at levels below the inversion, as can be diagnosed from Figs. 13e,f. Here the strongest tangential wind component increase occurs directly above the inversion, between 300 and 400 m, as was indicated by the observations (cf. Figs. 9–12).

Figures 14–19 depict a suite of TAPPS-generated products from the 12-km fine mesh simulations for use in the AVOSS, for each of the five deployment days at DFW. These simulations were all initialized at 0300 UTC from the coarse mesh 3-h simulated fields and integrated for 21 h of real time. The coarse mesh model was initialized from conventional observations valid at 0000 UTC on each of these 5 days and integrated for 24 h of real time. The five products, each displayed in time–height format, include 1)  $u$  (cross-runway) wind velocity component, 2) vertical shear of the cross-runway wind velocity component, 3) virtual potential temperature, 4) Richardson number and TKE, and 5) EDR. These simulations unambiguously show 1) the dominance of the DPBLJ signal during this 5-day period, 2) the day to day similarity in the evolution of each

Figures 14–19 depict a suite of TAPPS-generated products from the 12-km fine mesh simulations for use in the AVOSS, for each of the five deployment days at DFW. These simulations were all initialized at 0300 UTC from the coarse mesh 3-h simulated fields and integrated for 21 h of real time. The coarse mesh model was initialized from conventional observations valid at 0000 UTC on each of these 5 days and integrated for 24 h of real time. The five products, each displayed in time–height format, include 1)  $u$  (cross-runway) wind velocity component, 2) vertical shear of the cross-runway wind velocity component, 3) virtual potential temperature, 4) Richardson number and TKE, and 5) EDR. These simulations unambiguously show 1) the dominance of the DPBLJ signal during this 5-day period, 2) the day to day similarity in the evolution of each

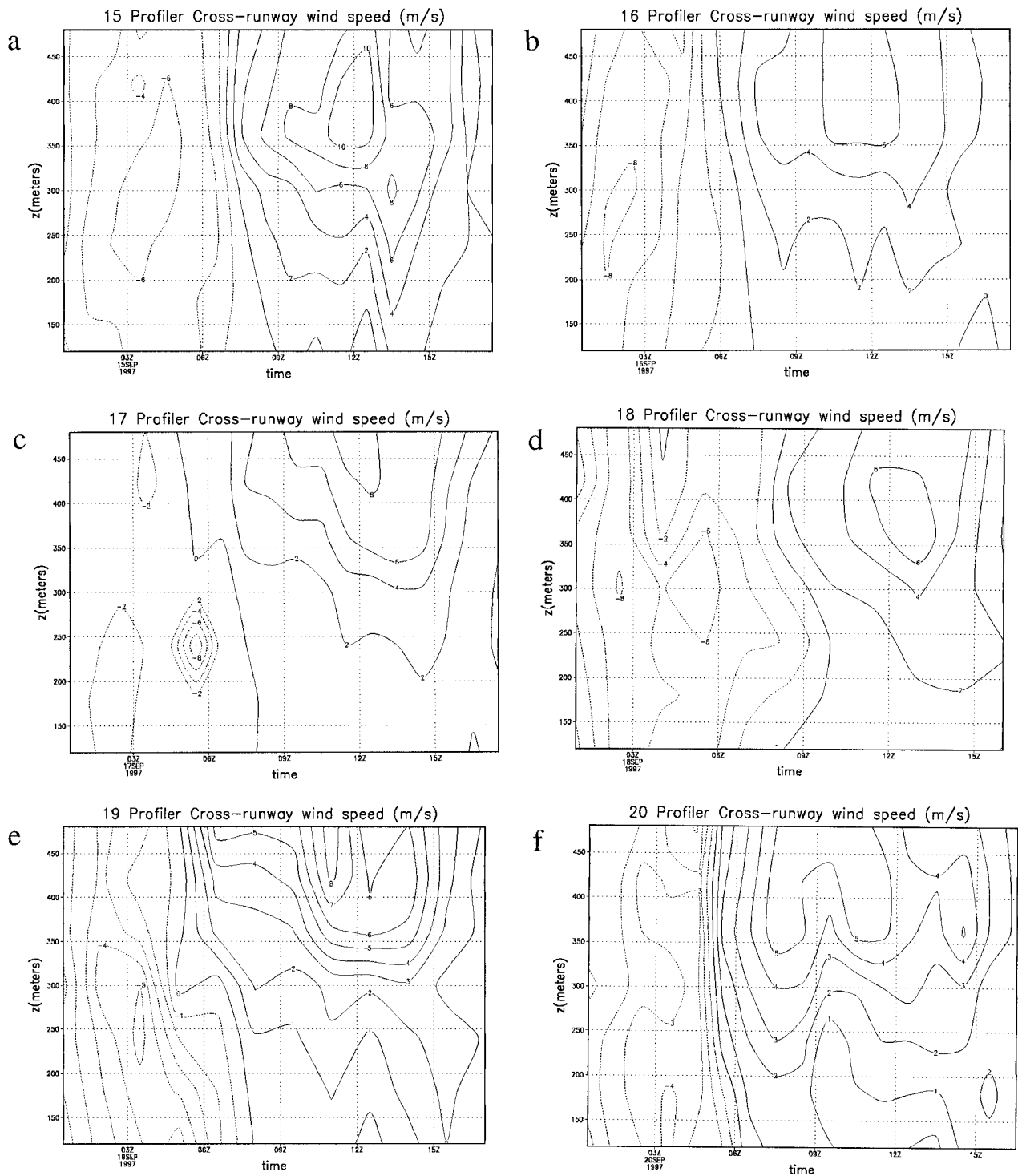
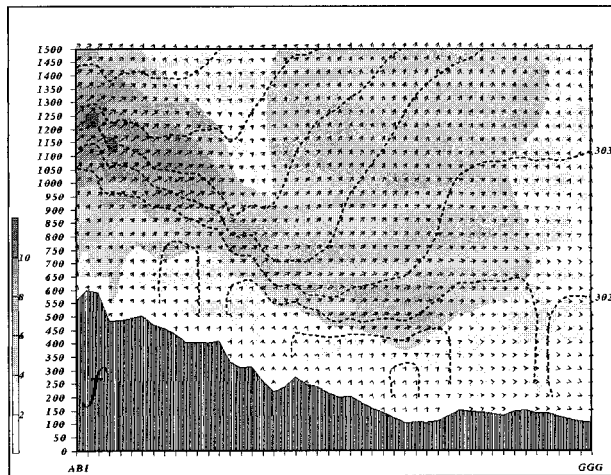
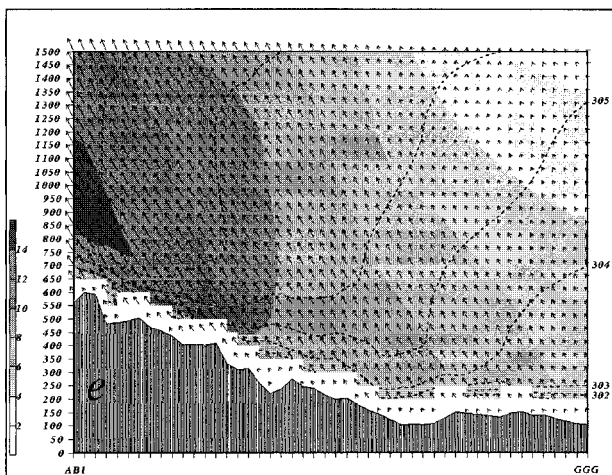
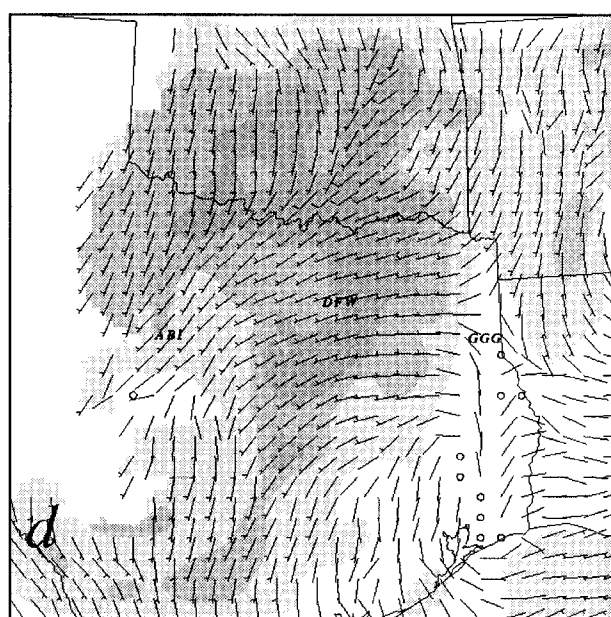
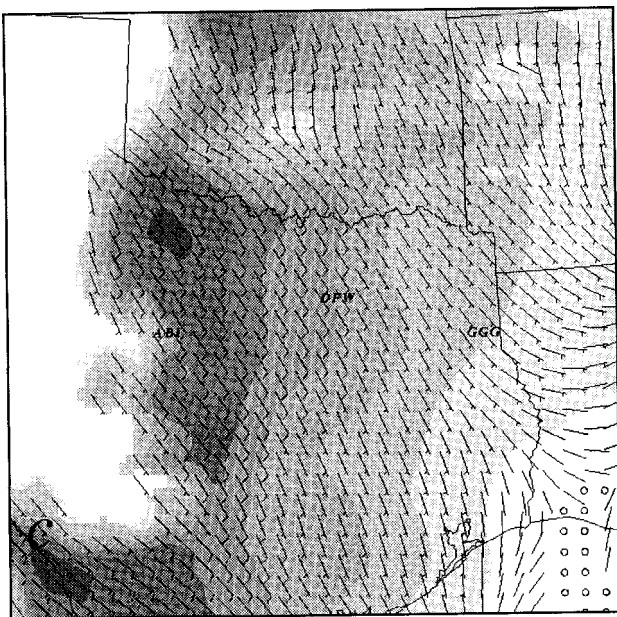
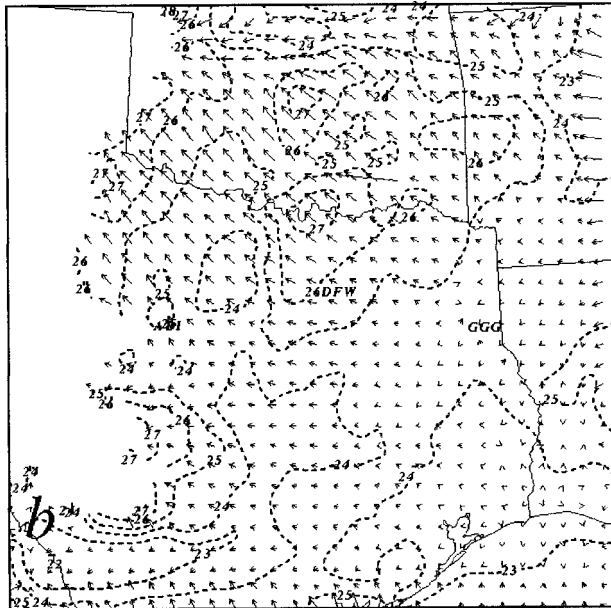
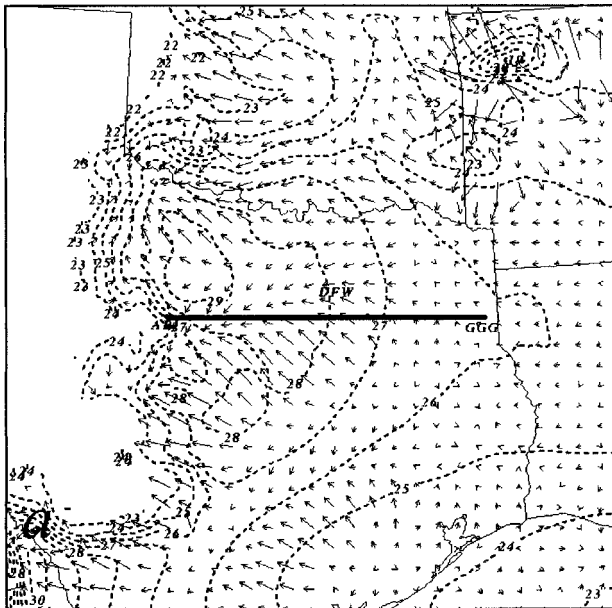


FIG. 12. DFW profiler-derived time–height (100–500 m = AGL) sections of cross-runway ( $u$ ) wind velocity component valid from 0000–1800 UTC on (a) 15 Sep 1997, (b) 16 Sep 1997, (c) 17 Sep 1997, (d) 18 Sep 1997, (e) 0000–2100 UTC on 19 Sep 1997, and (f) 0000–1800 UTC on 20 Sep 1997.

product, and 3) the importance of the DPBLJ in the derived turbulence products. All five case studies produce a clearly defined DPBLJ signal with the average statistics for the jet maximum shown in Table 4. These

average values of the simulated maximum jet structure can be compared to the observed average maximum values at all five locations (Table 3). Furthermore, a direct comparison, in sounding format, between



simulated cross-runway wind component values and observations at UTD and FWD is presented from a small sample in Fig. 19 and Table 5. The soundings indicate that the model has the ability to predict the vertical structure of the maxima, while the maxima comparisons assess the amplitude predictions. These comparisons indicate that representative errors between observed and simulated profiles of the cross-runway wind component maxima are on the order of  $1.2 \text{ m s}^{-1}$  for the most accurate 8- and 14-h forecasts, while errors in the height of the maximum cross-runway component are about 15 m. An additional gauge of the accuracy of the simulations can also be diagnosed by comparing profiler-derived values at DFW to simulated values from 15 September 1997. The profiler, which is located directly at DFW, is a more accurate indicator of the winds than rawinsondes, which can be significantly displaced from the simulated DFW values. Representative differences/model errors are typically on the order of  $1 \text{ m s}^{-1}$ , with the maximum temporally displaced by 15–30 min and an elevation displacement of about 30 m in the cross-runway wind component.

The maxima in TKE are, in most cases, roughly aligned with the maxima in cross-runway wind component, reflecting the strong vertical wind shear fields. The simulated EDRs, depicted in Fig. 18, reflect the shear fields as well but are also displaced to a slightly

later time, reflecting the importance of both increased vertical wind shear and buoyancy in dissipating atmospheric eddies. The maximum EDR values tend to occur near the surface and are generally on the order of  $0.02\text{--}0.05 \text{ m}^2 \text{ s}^3$ . It is not uncommon for the EDR

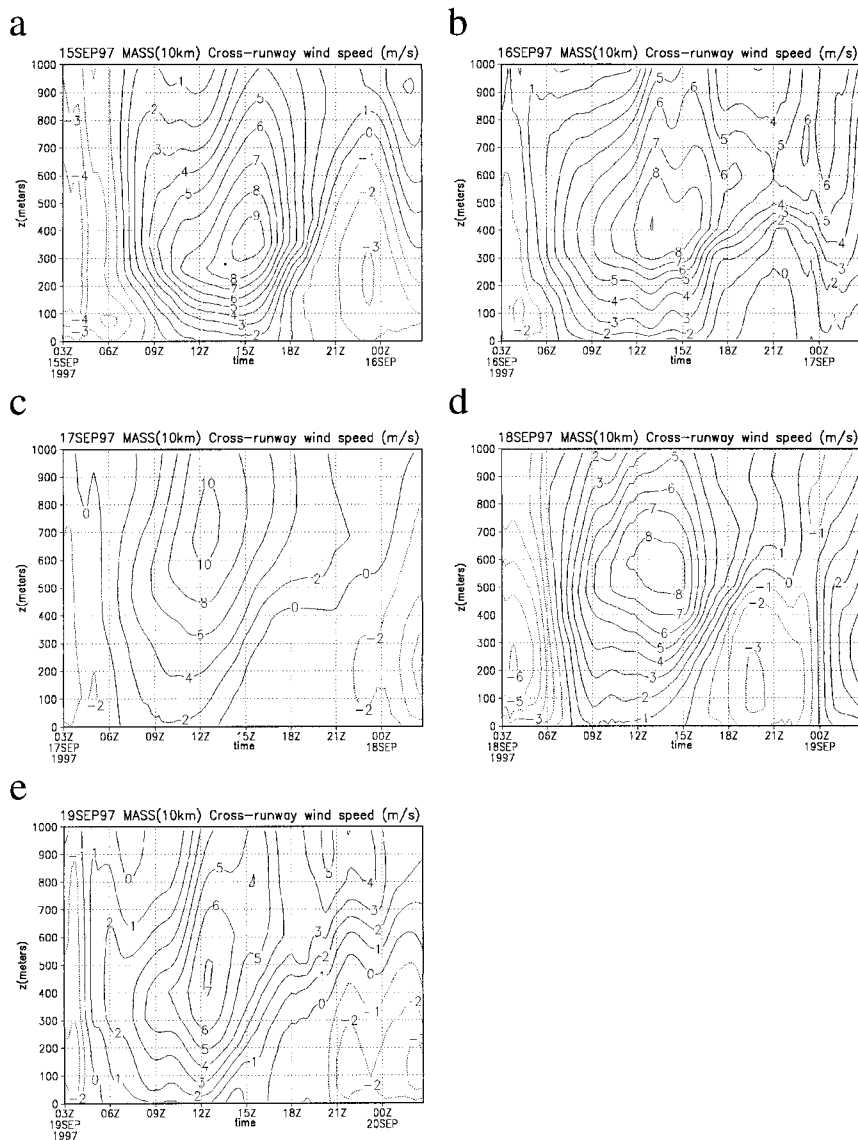


FIG. 14. TAPPS fine mesh simulated time–height (0–1000 m AGL) sections of cross-runway ( $u$ ) wind velocity component ( $\text{m s}^{-1}$ ) at DFW valid for 0300–0300 UTC on (a) 15–16 Sep 1997, (b) 16–17 Sep 1997, (c) 17–18 Sep 1997, (d) 18–19 Sep 1997, and (e) 19–20 Sep 1997.

FIG. 13. TAPPS fine mesh simulated pressure gradient force vectors and temperature (dashed, in  $^{\circ}\text{C}$ ) at 605 m above MSL valid at (a) 0300 and (b) 0900 UTC on 15 Sep 1997. TAPPS fine mesh simulated horizontal winds (wind barbs, with magnitude shaded in  $\text{m s}^{-1}$ ) on the 605 m MSL level valid at (c) 0300 and (d) 0900 UTC. TAPPS tangential wind velocity component (shaded in  $\text{m s}^{-1}$ ), potential temperature (solid in K), and cross-section winds (vectors) along a cross section from Abilene, TX (ABI), to Longview, TX (GGG), from the surface to 1500 m MSL valid at (e) 0300 and (f) 0900 UTC 15 Sep 1997. The thick solid line (a) indicates the location of the vertical cross section.

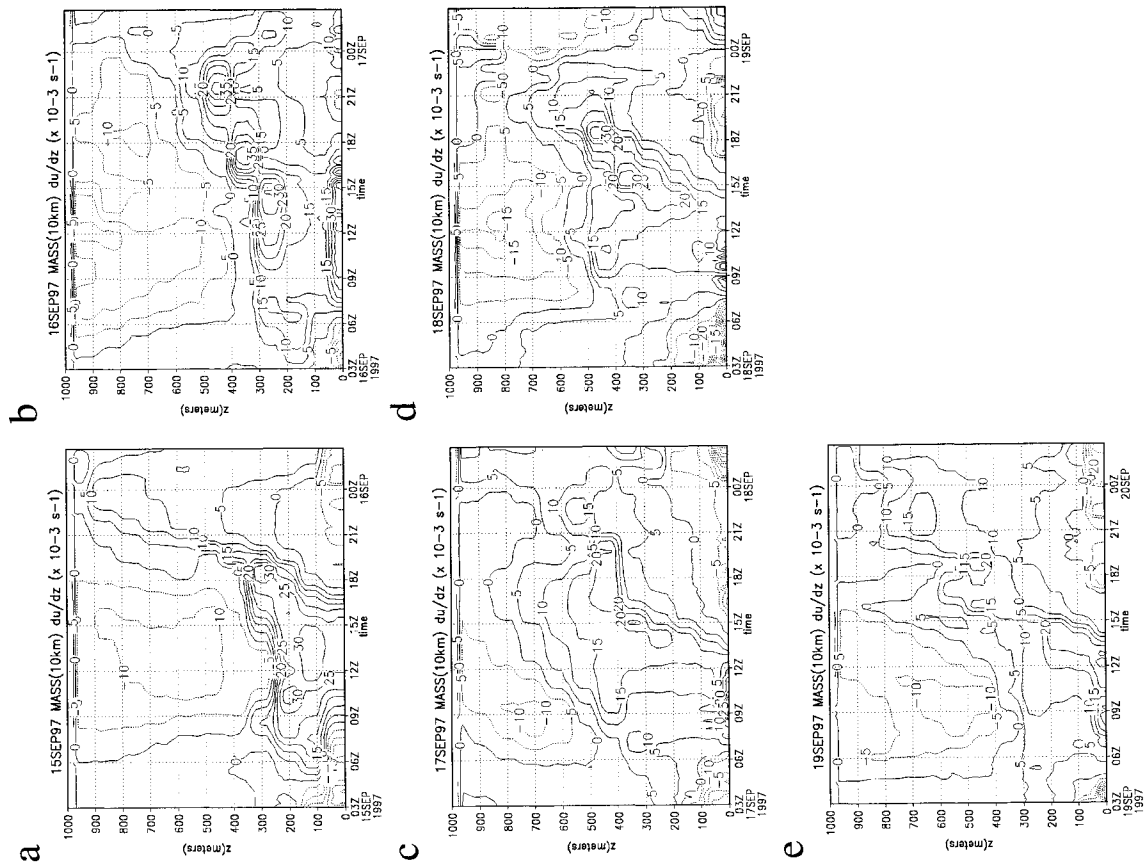
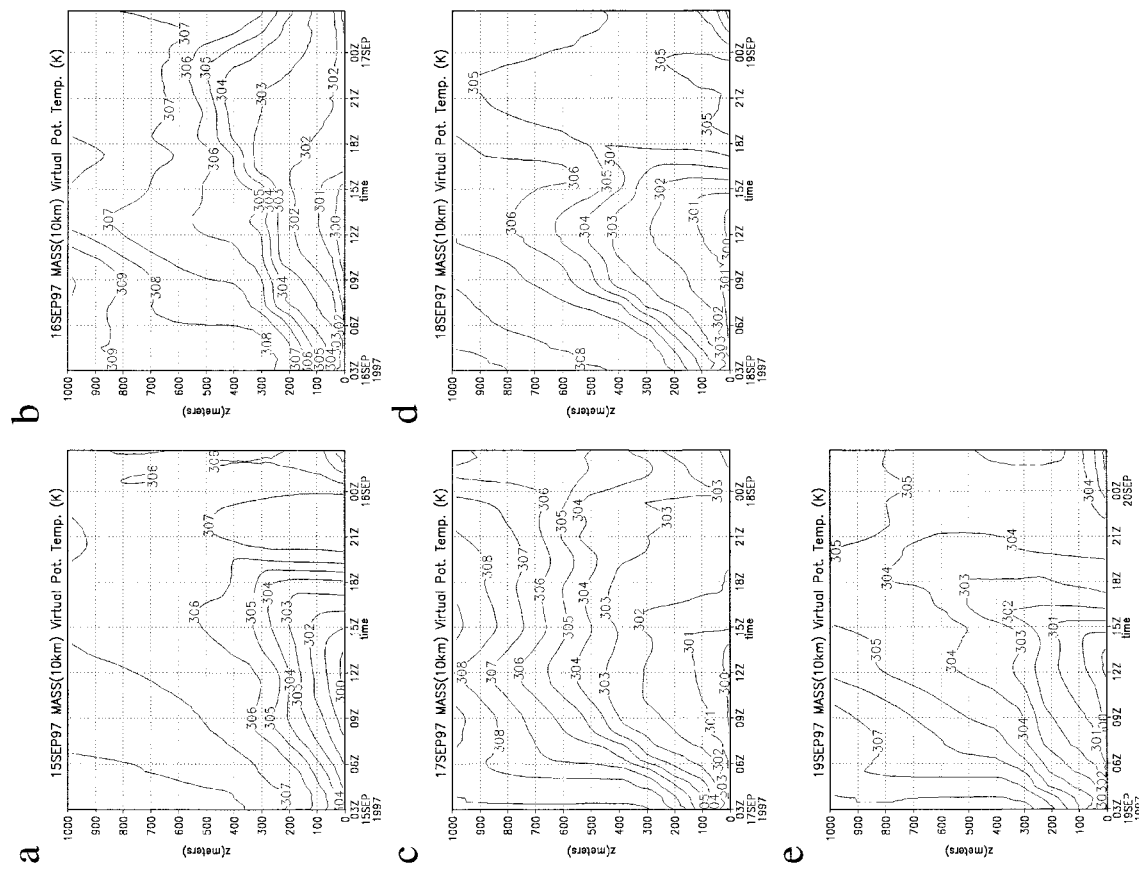


Fig. 15. TAPPS fine mesh simulated time-height (0–1000 m AGL) sections of vertical wind shear of the cross-runway ( $u$ ) wind velocity component ( $\times 10^{-3} \text{ s}^{-1}$ ) at DFW valid for 0300–0300 UTC on (a) 15–16 Sep 1997, (b) 16–17 Sep 1997, (c) 17–18 Sep 1997, (d) 18–19 Sep 1997, and (e) 19–20 Sep 1997.

Fig. 16. TAPPS fine mesh simulated time-height (0–1000 m AGL) sections of virtual potential temperature (K) at DFW valid for 0300–0300 UTC on (a) 15–16 Sep 1997, (b) 16–17 Sep 1997, (c) 17–18 Sep 1997, (d) 18–19 Sep 1997, and (e) 19–20 Sep 1997.



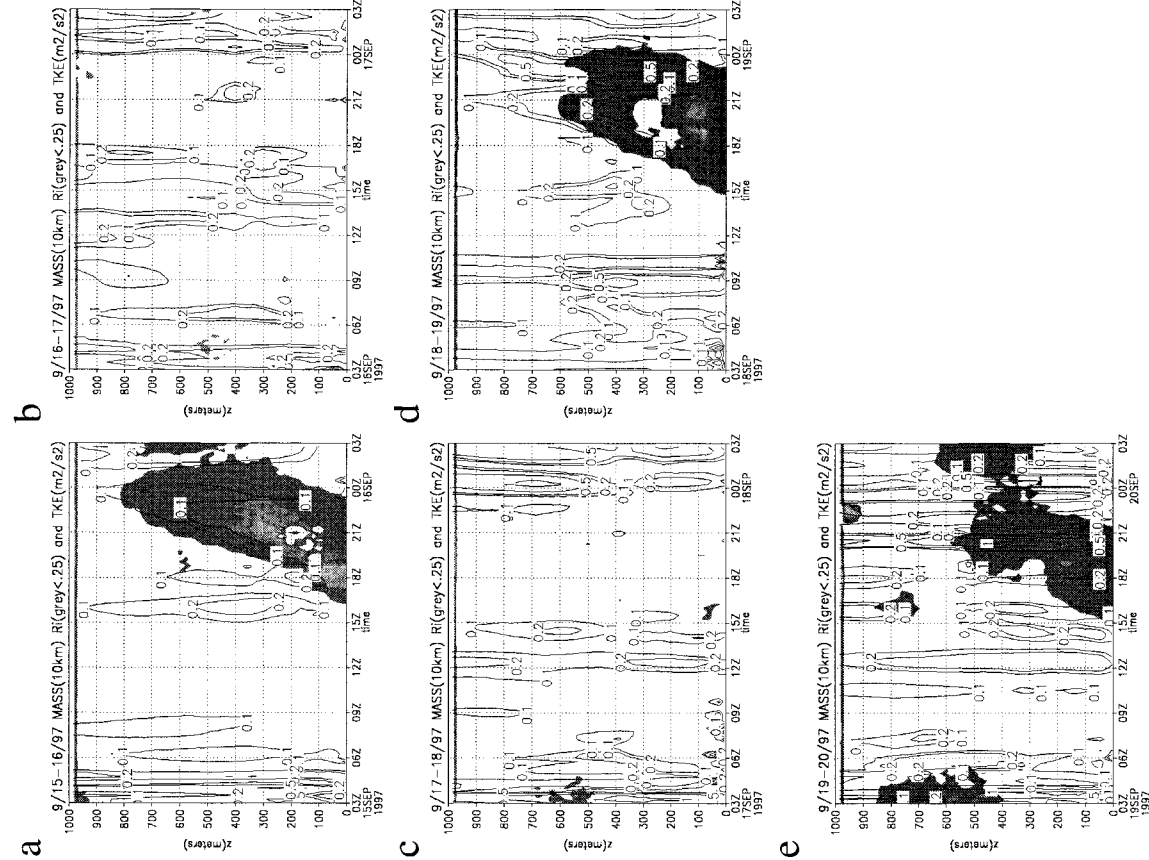


FIG. 17. TAPPS fine mesh simulated time-height (0–1000 m AGL) sections of Richardson number (shaded <math>< 0.25</math>) and turbulent kinetic energy (

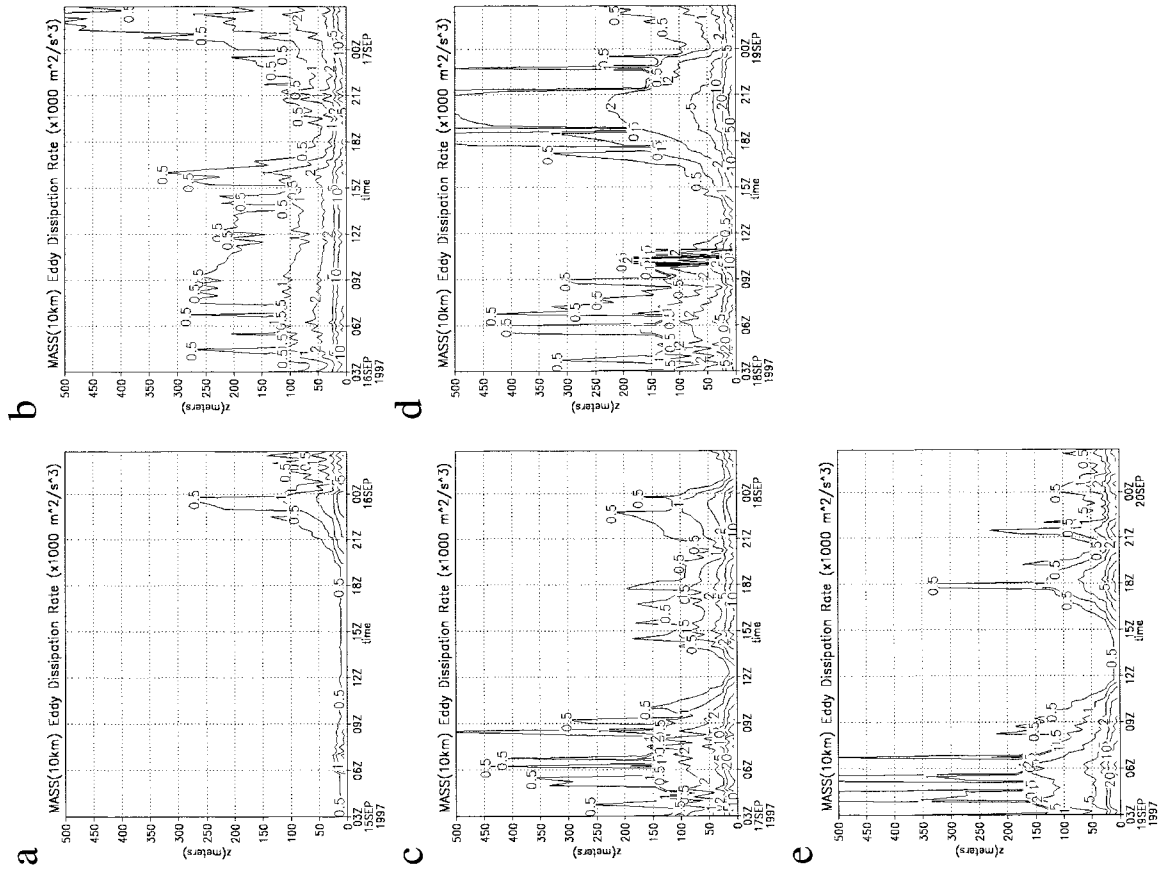


FIG. 18. TAPPS fine mesh simulated time-height (0–500 m AGL) sections of eddy dissipation rate ( $\times 10^4 \text{ m}^2 \text{ s}^{-3}</math>) at DFW valid for 0300–0300 UTC on (a) 15–16 Sep 1997, (b) 16–17 Sep 1997, (c) 17–18 Sep 1997, (d) 18–19 Sep 1997, and (e) 19–20 Sep 1997.$

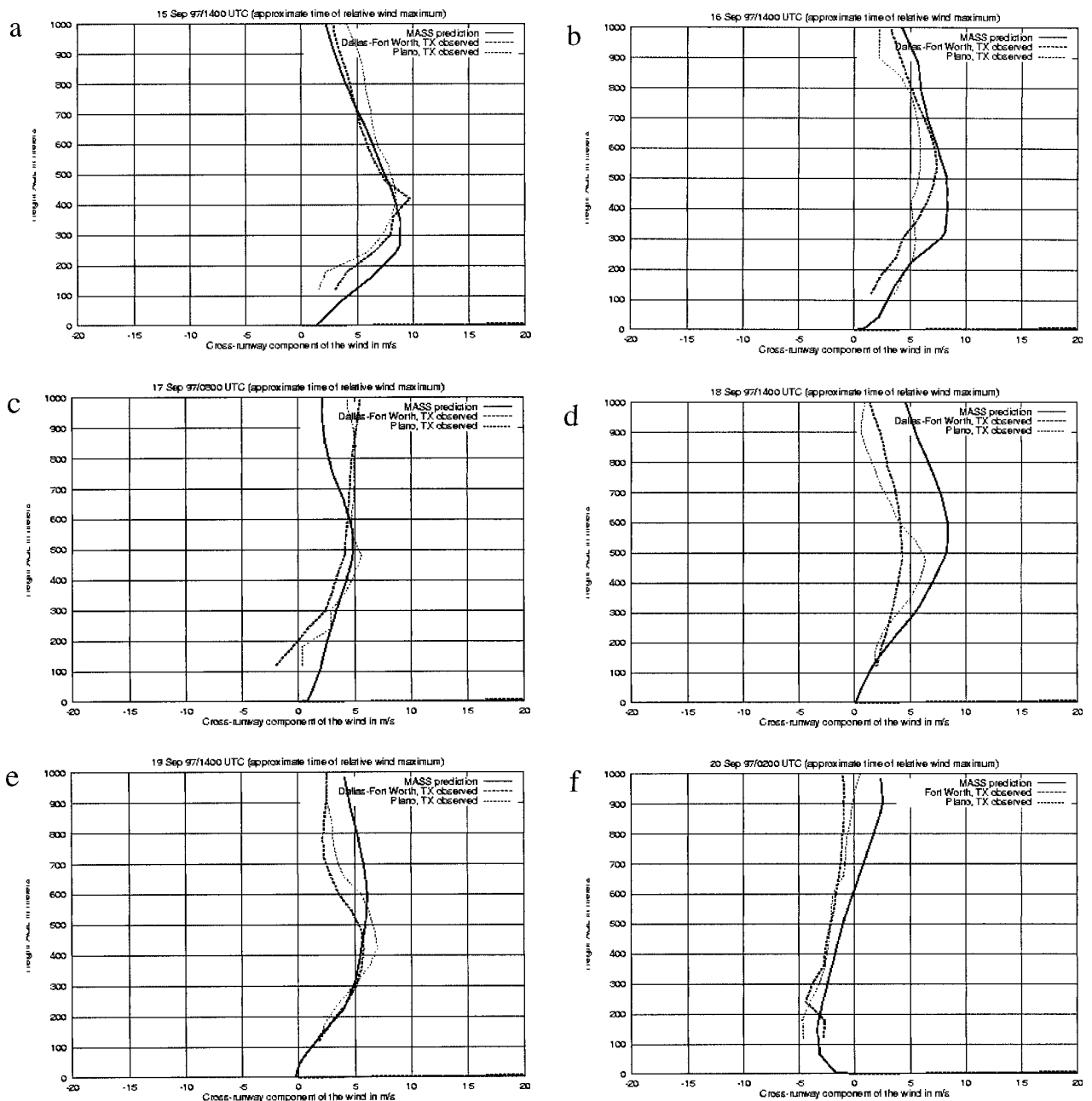


FIG. 19. TAPPS fine mesh simulated cross-runway ( $u$ ) wind component sounding (solid line in  $m\ s^{-1}$ ) valid at DFW vs Plano, TX (dotted line in  $m\ s^{-1}$ ), and Fort Worth, TX (dashed line in  $m\ s^{-1}$ ), observed cross-runway ( $u$ ) wind component valid at (a) 1400 UTC on 15 Sep 1997, (b) 1400 UTC on 16 Sep 1997, (c) 0800 UTC on 17 Sep 1997, (d) 1400 UTC on 18 Sep 1997, (e) 1400 UTC on 19 Sep 1997, and (f) 0200 UTC on 20 Sep 1997.

maxima to be split in time as there can be a substantial difference in time between the mechanically forced dissipation due to vertical wind shear and the buoyancy-forced dissipation several hours following the LLJ-induced shear maxima. Comparisons with observations from the DFW deployment (not shown) indicate that TAPPS EDRs, which are derived from higher-order closure simulations, capture the impor-

tant tendencies in the evolving observed EDR fields. However, TAPPS EDRs do tend to slightly overestimate the effects of DPBLJ-induced vertical wind shears during the early morning, and to slightly underestimate the effects of surface heating-induced buoyancy during the afternoon. Further refinements in the TAPPS turbulence diagnostics are on going, and will be included in TAPPS-2 for the DFW 2000 demo.

TABLE 4. A comparison between the observed LLJ at Plano and Fort Worth, and the MASS 12-km simulated LLJ at DFW. Magnitudes ( $\text{m s}^{-1}$ ) and height (m) of the LLJ are shown from 15 to 20 Sep 1997.

MASS 5.10 10-km simulated LLJs at DFW vs Plano and Fort Worth observed LLJs				
Day (Sep 1997)	Time (UTC)	MASS ( $\text{m s}^{-1}$ )	Plano ( $\text{m s}^{-1}$ )	Fort Worth ( $\text{m s}^{-1}$ )
15	1400	8.5 at 300m	8.0 at 410m	9.5 at 425m
16	1400	8.5 at 400m	6.0 at 300m	8.3 at 500m
17	0800	5.0 at 500m	5.5 at 475m	4.8 at 500m
18	1400	8.5 at 550m	6.0 at 475m	3.0 at 500m
19	1400	6.5 at 600m	7.0 at 425m	5.5 at 400m
20	0200	-3.0 at 150m	-4.9 at 175m	-4.8 at 250m
Avg (six case studies)		5.7 at 417m	4.6 at 377m	4.4 at 429m

The products generated by TAPPS will be employed in the AVOSS, which will be running operationally at DFW during the year 2000 demonstration. The AVOSS requires information on stability, cross-wind component velocity, vertical wind shear, TKE, and EDR to determine appropriate safe spacing between aircraft. The algorithms in AVOSS will assimilate these forecasts from TAPPS and build them into the automated product coming out of AVOSS.

#### 4. Summary and conclusions

An operational numerical weather prediction system, TAPPS, has been described in an in-depth manner. This system comprises a data ingestion system, a mesoscale numerical model, and a postprocessing system whose focus is to develop products for short-term PBL applications. The system is presently being evaluated for its utility in supporting AVOSS at DFW in preparation for the formal AVOSS demonstration. It is anticipated that the existing version of TAPPS (TAPPS-1), which utilizes conventional synoptic-scale observations, will be improved to employ asynoptic datasets for shorter-period, higher-resolution simulations in the near future. The TAPPS products focus on time-height sections and vertical sounding profiles of cross-runway wind component, headwind component, wind statistics, potential temperature, Richardson number,

TKE, and EDR. Comparisons between asynoptic balloon and profiler observations and model-generated products for a 5-day period, during which a persistent diurnally forced PBL jet was observed, indicate that the forecast system can accurately replicate the jet stream evolution. Small errors in jet stream structure, maximum velocity, and time of arrival were found at several point locations. Since nocturnal jets are likely a highly ubiquitous phenomena, particularly where terrain and surface characteristic variations occur, this prototype system will likely be expanded for operational use at most North American airport terminals,

TABLE 5. A comparison between average characteristics of the MASS 5.10 12-km simulated LLJs and the observed LLJs.

	Simulated	Observed
Jet maximum period	~1230–1430 UTC	~1330 UTC
Level of jet maximum	~500 m AGL	~550 m AGL
Jet maximum velocity	~8.0 $\text{m s}^{-1}$	~7.0 $\text{m s}^{-1}$
Shear maximum	~ $2.6 \times 10^{-2} \text{ s}^{-1}$	~ $2.9 \times 10^{-2} \text{ s}^{-1}$
Level of maximum shear	~245 m AGL	~200–300 m AGL
Inversion layer	~120–450 m AGL	~300–555 m AGL
TKE maximum time	~1500 UTC	
Level of TKE maximum	~500 m AGL	
TKE maximum	~0.2 $\text{m}^2 \text{ s}^{-2}$	

should AVOSS be deployed elsewhere in the future. Furthermore, it has the potential for application to *en route* aviation weather forecast problems, such as clear air and convective turbulence as well as icing and visibility above the PBL.

*Acknowledgments.* This research is being supported by NASA's Terminal Area Productivity Program under Cooperative Agreement NCC-1-220 that is being managed by the NASA Langley Research Center. The authors would like to thank the NASA contract monitor, Dr. Fred H. Proctor, for his technical and administrative support, as well as insightful comments on the final manuscript. Additionally, David A. Hinton, the AVOSS principal investigator, and R. Brad Perry, the reduced separation and operations manager, of the NASA Langley Flight Dynamics and Control Division, provided support and helpful comments on numerous occasions. We would also like to thank Jennifer Kehoe and Christopher Hill for their help in preparing the figures for this manuscript. Many individuals contributed to the organization, implementation, and execution of the DFW deployment synoptic rawinsonde observational network. These include Les Showell and David Rust of NOAA/NSSL; J. Allen Zak of Vigyan Inc.; Michael Matthews, Kim Theriault, and Glenn Perras of MIT Lincoln Laboratory; Prof. John Hoffman of the University of Texas at Dallas; Prof. Duncan Weathers of the University of North Texas; Ken Williams of the Waxahatchie, Texas, regional airport; Donald Penny and Tim Miller of the NASA Wallops Space Flight Center; and Skip Eli and Donny Sullivan of the Fort Worth, Texas, NWS Forecast Office. Captain Daniel A. Shaltanis of the United States Air Force modified the profiler data ingestion and analysis system under development in TAPPS. Li Zhao of North Carolina State University helped generate many of the model and observational figures in this paper. Dr. Kenneth T. Waight III of MESO, Inc., provided guidance with the MASS model. Computing was performed on the dedicated TAPPS DEC-ALPHA 600 system at the Department of Marine, Earth, and Atmospheric Sciences of North Carolina State University.

## References

- Anderson, J. R., E. E. Hardy, J. T. Roach, and R. E. Witmer, 1976: A land use and land over classification system for use with remote sensor data. U.S. Geological Survey Professional Paper 964, U.S. Government Printing Office, Washington, DC, 28 pp. [Available from U.S. Government Printing Office, Washington, DC 20402.]
- Arritt, R. W., T. D. Rink, M. Segal, D. P. Todey, and C. A. Clark, 1997: The Great Plains low-level jet during the warm season of 1993. *Mon. Wea. Rev.*, **125**, 2176–2192.
- Arya, S. P., 1988: *Introduction to Micrometeorology*. Academic Press, 307 pp.
- Bauman, W. H., III, M. L. Kaplan, and S. Businger, 1997: Nowcasting convective activity for space shuttle landings during easterly flow regimes. *Wea. Forecasting*, **12**, 79–107.
- Blackadar, A. K., 1957: Boundary layer and maxima and their significance for the growth of nocturnal inversions. *Bull. Amer. Meteor. Soc.*, **38**, 283–290.
- , 1979: High resolution models of the planetary boundary layer. *Advances in Environmental Science and Engineering*, J. Pfafflin and E. Ziegler, Eds., Vol. 1, Gordon and Breach, 50–85.
- Bluestein, H. B., 1993: *Synoptic-Dynamic Meteorology in Midlatitudes*. Vol. II. Oxford University Press, 594 pp.
- Bonner, W. D., 1968: Climatology of the low-level jet. *Mon. Wea. Rev.*, **96**, 833–850.
- Carpenter, R. L., Jr., K. K. Drogemeier, P. R. Woodward, and C. E. Hane, 1988: Application of the piecewise parabolic method (PPM) to meteorological modeling. Preprints, *Eighth Conf. on Numerical Weather Prediction*, Baltimore, MD, Amer. Meteor. Soc., 791–798.
- Cram, J. M., and M. L. Kaplan, 1985: Variational assimilation of VAS data into a mesoscale model: Assimilation method and sensitivity experiments. *Mon. Wea. Rev.*, **113**, 467–484.
- , ——, C. A. Mattocks, and J. W. Zack, 1991: The use and analysis of profiler winds to derive mesoscale height and temperature fields: Simulation and real data experiments. *Mon. Wea. Rev.*, **119**, 1041–1056.
- Daley, R., 1992: *Atmospheric Data Analysis*. Cambridge University Press, 457 pp.
- Dasey, T. J., R. E. Cole, R. M. Heinrichs, M. P. Mathews, and G. H. Perras, 1998: Aircraft Vortex Spacing System (AVOSS) initial 1997 system deployment at Dallas/Ft. Worth (DFW) airport. Project Rep. NASA/L-3, 68 pp. [Available from MIT Lincoln Laboratory, Lexington, MA 02420.]
- Davies, H. C., 1976: A lateral boundary formulation for multi-level prediction models. *Quart. J. Roy. Meteor. Soc.*, **102**, 405–418.
- Fast, J. D., and M. D. McCorkle, 1990: A two-dimensional numerical sensitivity study of the Great Plains low-level jet. *Mon. Wea. Rev.*, **118**, 151–163.
- Hamilton, D. W., Y.-L. Lin, R. P. Weglarz, and M. L. Kaplan, 1998: Jetlet formation from diabatic forcing with applications to the 1994 Palm Sunday tornado outbreak. *Mon. Wea. Rev.*, **126**, 2061–2089.
- Han, J., Y.-L. Lin, S. P. Arya, and F. H. Proctor, 1999: Large eddy simulation of aircraft wake vortices in a homogeneous atmospheric turbulence: Vortex decay and descent. Preprints, *37th Aerospace Sciences Meeting and Exhibit*, Reno, NV, AIAA Paper 99-0756, American Institute of Aeronautics and Astronautics, 21 pp.
- Hinton, D. A., 1995: Aircraft Vortex Spacing System (AVOSS) Conceptual Design. NASA Tech. Memo. 110184, 32 pp. [Available from NASA Langley Research Center, Hampton, VA 23681.]
- , 1996: An aircraft vortex spacing system (AVOSS) for dynamical wake vortex spacing criteria. Preprints, *AGARD 78th Fluid Dynamics Panel Meeting and Symp.*, Trondheim, Norway, AGARD CP-584, Paper 23, Advisory Group for Aerospace Research and Development, 11 pp.
- , J. K. Charnock, D. R. Bagwell, and D. Grigsby, 1999: NASA Aircraft Vortex Spacing System development status. Preprints, *37th Aerospace Sciences Meeting and Exhibit*, Reno, NV, AIAA Paper 99-0753, American Institute of Aeronautics and Astronautics, 17 pp.
- Kain, J. S., and J. M. Fritsch, 1990: A one-dimensional entraining/detraining plume model. *J. Atmos. Sci.*, **47**, 2784–2802.
- Kaplan, M. L., and V. M. Karyampudi, 1992a: Meso-beta scale numerical simulations of terrain drag-induced along-stream

- circulations. Part I: Midtropospheric frontogenesis. *Meteor. Atmos. Phys.*, **49**, 133–156.
- , and —, 1992b: Meso-beta scale numerical simulations of terrain drag-induced along-stream circulations. Part II: Concentration of potential vorticity within dryline bulges. *Meteor. Atmos. Phys.*, **49**, 157–185.
- , J. W. Zack, V. C. Wong, and J. J. Tuccillo, 1982a: Initial results from a mesoscale atmospheric simulation system and comparisons with the AVE-SESAME I data set. *Mon. Wea. Rev.*, **110**, 1564–1590.
- , —, —, and —, 1982b: A sixth-order mesoscale atmospheric simulation system applicable to research and real-time mesoscale forecasting problems. *Symposium on Mesoscale Modeling*, Y. Sasaki, Ed., Cooperative Institute for Mesoscale Meteorological Studies, 38–84.
- , —, —, and G. D. Coats, 1983: A nested-grid mesoscale numerical weather prediction model modified for Space Shuttle operational requirements. Preprints, *Ninth Conf. on Aerospace and Aeronautical Meteorology*, Omaha, NE, Amer. Meteor. Soc., 341–347.
- , —, —, J. J. Tuccillo, and G. D. Coats, 1984: The interactive role of subsynoptic scale jet streak and planetary boundary layer processes in organizing an isolated convective complex. *Mon. Wea. Rev.*, **112**, 2212–2237.
- , R. A. Rozumalski, R. P. Weglarz, Y.-L. Lin, S. Businger, and R. F. Gonski, 1995: Numerical simulation studies of the mesoscale environment conducive to the Raleigh tornado. NOAA Tech. Memo. NWS ER-90, 101 pp. [Available from National Weather Service, Raleigh Forecast Office, 1005 Capability Dr., Raleigh, NC 27695.]
- , S. E. Koch, Y.-L. Lin, R. P. Weglarz, and R. A. Rozumalski, 1997: Numerical simulations of a gravity wave event over CCOPE. Part I: The role of geostrophic adjustment in mesoscale jetlet formation. *Mon. Wea. Rev.*, **125**, 1185–1211.
- , Y.-L. Lin, D. W. Hamilton, and R. A. Rozumalski, 1998: The numerical simulation of an unbalanced jetlet and its role in the Palm Sunday 1994 tornado outbreak in Alabama and Georgia. *Mon. Wea. Rev.*, **126**, 2133–2165.
- , R. P. Weglarz, Y.-L. Lin, D. B. Ensley, J. K. Kehoe, and D. S. Decroix, 1999: A terminal area PBL prediction system for DFW. Preprints, *37th Aerospace Sciences Meeting and Exhibit*, Reno, NV, AIAA Paper No. 99-0983, American Institute of Aeronautics and Astronautics, 27 pp.
- Koch, S. E., 1985: Ability of a regional scale model to predict the genesis of intense mesoscale convective systems. *Mon. Wea. Rev.*, **113**, 1693–1713.
- , W. C. Skillman, P. J. Kocin, P. J. Wetzel, K. Brill, D. A. Keyser, and M. C. McCumber, 1983: Evaluation of the synoptic and mesoscale predictive capabilities of a mesoscale atmospheric simulation system. NASA Tech. Memo. 84995, 104 pp. [Available from Goddard Space Flight Center, Greenbelt, MD 20771.]
- , —, —, —, —, —, and —, 1985: Synoptic scale forecast skill and systematic errors in the MASS 2.0 model. *Mon. Wea. Rev.*, **113**, 1714–1737.
- , D. W. Hamilton, D. Kramer, and A. Langmaid, 1998: Mesoscale dynamics in the Palm Sunday tornado outbreak. *Mon. Wea. Rev.*, **126**, 2031–2060.
- Kocin, P. J., L. W. Uccellini, J. W. Zack, and M. L. Kaplan, 1984: Recent examples of mesoscale numerical forecasts of severe weather events along the East Coast. NASA Tech. Memo. 86172, 57 pp. [Available from NASA Goddard Space Flight Center, Greenbelt, MD 20771.]
- , —, —, and —, 1985: Mesoscale numerical simulations of severe weather events along the East Coast. *Bull. Amer. Meteor. Soc.*, **66**, 1412–1424.
- Lin, Y.-L., R. D. Farley, and H. D. Orville, 1983: Bulk parameterization of the snow field in a cloud model. *J. Climate Appl. Meteor.*, **22**, 1065–1092.
- Mahrt, L., and H. Pan, 1984: A two-layer model of soil hydrology. *Bound.-Layer Meteor.*, **29**, 1–20.
- Manobianco, J., L. W. Uccellini, K. F. Brill, and P. J. Kocin, 1991: Contrasting the impact of dynamic data assimilation on the numerical simulation of cyclogenesis during GALE IOP 10 and IOP 1. *Meteor. Atmos. Phys.*, **45**, 41–63.
- , —, —, and Y.-H. Kuo, 1992: The impact of dynamic data assimilation on the numerical simulations of the *QE II* cyclone and an analysis of the jet streak influencing the precyclogenetic environment. *Mon. Wea. Rev.*, **120**, 1973–1996.
- , S. E. Koch, V. M. Karyampudi, and A. J. Negri, 1994: The impact of assimilating satellite-derived precipitation rates on numerical simulations of the ERICA IOP-4 cyclone. *Mon. Wea. Rev.*, **122**, 341–365.
- , J. W. Zack, and G. E. Taylor, 1996: Workstation-based real-time mesoscale modeling designed for weather support operations at the Kennedy Space Center and Cape Canaveral Air Station. *Bull. Amer. Meteor. Soc.*, **77**, 653–672.
- Mass, C. F., and Y.-H. Kuo, 1998: Regional real-time numerical weather prediction: Current status and future potential. *Bull. Amer. Meteor. Soc.*, **79**, 253–263.
- McCorkle, M. D., 1988: Simulation of surface-moisture effects on the Great Plains low-level jet. *Mon. Wea. Rev.*, **116**, 1705–1720.
- McNider, R. T., and R. A. Pielke, 1981: Diurnal boundary-layer development over sloping terrain. *J. Atmos. Sci.*, **38**, 2198–2212.
- Mesinger, F., 1977: Forward-backward scheme and its use in a limited area model. *Contrib. Atmos. Phys.*, **50**, 200–210.
- , and A. Arakawa, 1977: Numerical methods used in atmospheric models. Garp Publication Series 17, Vol. 1, World Meteorological Organization, 64 pp.
- MESO, Inc., 1995: MASS reference manual. Version 5.10. 129 pp. [Available from MESO, Inc., 185 Jordan Road, Troy, NY 12180.]
- Mitchell, M. J., R. W. Arritt, and K. Labas, 1995: A climatology of the warm season Great Plains low-level jet using wind profiler observations. *Wea. Forecasting*, **10**, 576–591.
- Noilhan, J., and S. Planton, 1989: A simple parameterization of land surface processes for meteorological models. *Mon. Wea. Rev.*, **117**, 536–549.
- Perry, R. P., D. A. Hinton, and R. A. Stuever, 1997: NASA wake vortex research for aircraft spacing. Preprints, *35th Aerospace Sciences Meeting and Exhibit*, Reno, NV, AIAA Paper 97-0057, American Institute of Aeronautics and Astronautics, 9 pp.
- Proctor, F. H., 1998: The NASA-Langley wake vortex modelling effort in support of an operational aircraft spacing system. Preprints, *36th Aerospace Sciences Meeting and Exhibit*, Reno, NV, AIAA Paper 98-0589, American Institute of Aeronautics and Astronautics, 19 pp.
- Rogers, E., T. L. Black, D. G. Deaven, and G. J. DiMego, 1996: Changes to the operational “early” ETA analysis/forecast sys-

- tem at the National Centers for Environmental Prediction. *Wea. Forecasting*, **11**, 391–413.
- Sarpkaya, T., 1998: Decay of wake vortices of large aircraft. *AIAA J.*, **36**, 1671–1679.
- Stauffer, D. R., and N. L. Seaman, 1990: User of four-dimensional data assimilation in a limited-area mesoscale model. Part I: Experiments with synoptic-scale data. *Mon. Wea. Rev.*, **118**, 1250–1277.
- Stull, R. B., 1988: *An Introduction to Boundary Layer Meteorology*. Kluwer, 666 pp.
- Therry, G., and P. Lacarrere, 1983: Improving the eddy kinetic energy model for the planetary boundary layer. *Bound.-Layer Meteor.*, **25**, 63–88.
- Tombach, I., 1973: Observations of atmospheric effects on vortex wake behavior. *J. Aircr.*, **10**, 641–647.
- Tripoli, G. J., and W. R. Cotton, 1989: Numerical study of an observed orogenic mesoscale convective system. Part I: Simulated genesis and comparisons with observations. *Mon. Wea. Rev.*, **117**, 273–304.
- Uccellini, L. W., 1990: Processes contributing to the rapid development of extratropical cyclones. *Extratropical Cyclones—The Erik Palmén Memorial Volume*, C. W. Newton and E. O. Holopainen, Eds., Amer. Meteor. Soc., 81–105.
- , and D. R. Johnson, 1979: The coupling of upper- and lower-tropospheric jet streaks and implications for the development of severe convective storms. *Mon. Wea. Rev.*, **107**, 662–673.
- , K. F. Brill, R. A. Petersen, D. Keyser, R. Aune, P. J. Kocin, and M. des Jardins, 1986: A report on the upper-level wind conditions preceding and during the Shuttle Challenge (STS 51L) Explosion. *Bull. Amer. Meteor. Soc.*, **67**, 1248–1265.
- , R. A. Petersen, K. F. Brill, P. J. Kocin, and J. J. Tuccillo, 1987: Synergistic interactions between an upper-level jet streak and diabatic processes that influence the development of a low-level jet and a secondary coastal cyclone. *Mon. Wea. Rev.*, **115**, 2227–2261.
- Wexler, H., 1961: A boundary layer interpretation of the low-level jet. *Tellus*, **13**, 368–378.
- Whitaker, J. S., L. W. Uccellini, and K. F. Brill, 1988: A model-based diagnostic study of the explosive development phase of the Presidents' Day cyclone. *Mon. Wea. Rev.*, **116**, 2337–2365.
- Whiteman, C. D., X. Bian, and S. Zhong, 1997: Low-level jet climatology from enhanced rawinsonde observations at a site in the southern Great Plains. *J. Appl. Meteor.*, **36**, 1363–1376.
- Young, S., and J. W. Zack, 1998: A comparison of two 4-dimensional data (FDDA) assimilation schemes: Newtonian relaxation and incremental analysis updates. Preprints, *12th Conf. on Numerical Weather Prediction*, Phoenix, AZ, Amer. Meteor. Soc., 45–48.
- Zack, J. W., and M. L. Kaplan, 1987: Numerical simulations of the subsynoptic features associated with the AVE-SESAME I case. Part I: The preconvective environment. *Mon. Wea. Rev.*, **115**, 2367–2394.
- , V. M. Karyampudi, C. A. Mattocks, and G. D. Coats, 1988: Meso-beta scale simulations of convective cloud systems over Florida utilizing data derived from GOES satellite imagery. Preprints, *Eighth Conf. on Numerical Weather Prediction*, Baltimore, MD, Amer. Meteor. Soc., 293–300.
- Zhang, D.-L., and R. A. Anthes, 1982: A high-resolution model of the planetary boundary layer—Sensitivity tests and comparisons with SESAME-79 data. *J. Appl. Meteor.*, **21**, 1594–1609.

